RHEOLOGIC AND FLUME EROSION CHARACTERISTICS OF GEORGIA SEDIMENTS FROM BRIDGE FOUNDATIONS

A Thesis
Presented to
The Academic Faculty

by

Paul Myron Hobson

In Partial Fulfillment
of the Requirements for the Degree
Masters of Science in
Civil Engineering

School of Civil and Environmental Engineering
Georgia Institute of Technology
December 2008

RHEOLOGIC AND FLUME EROSION CHARACTERISTICS OF GEORGIA SEDIMENTS FROM BRIDGE FOUNDATIONS

Approved by:

Professor Terry W. Sturm, Advisor
School of Civil and Environmental Engineering
Georgia Institute of Technology

Professor Donald R. Webster
School of Civil and Environmental Engineering
Georgia Institute of Technology

Professor Susan E. Burns
School of Civil and Environmental Engineering
Georgia Institute of Technology

Date Approved: November 17, 2008

ACKNOWLEDGEMENTS

I would like to extend the most sincere gratitude to Dr. Terry Sturm for his unwavering guidance, wisdom, and support throughout this project. The input and feedback from Dr. Susan Burns and Dr. Donald Webster are also greatly appreciated. The laboratory work supporting this thesis would not have been possible without the assistance and expertise of Andy Udell. I would also like to thank Patti, Chris, and Shanna Hobson for their unending love and encouragement. Lastly, I am grateful for the support and patience of Eric Strecker and everyone at Geosyntec Consultants.

The funding and soil cores used to execute this project were provided by the Georgia Department of Transportation.

TABLE OF CONTENTS

LIST OF TABLES

LIST OF FIGURES

LIST OF SYMBOLS OR ABBREVIATIONS

A_c	Coefficient in equation to predict Shields parameter.
A_y	Coefficient in equation to predict dimensionless yield stress.
B_c	Coefficient in equation to predict Shields parameter.
C_c	Coefficient in equation to predict Shields parameter.
C_p	Mallow's C_p.
C_y	Coefficient in equation to predict dimensionless yield stress.
d_*	Dimensionless particle diameter.
d_{50}	Median particle diameter.
E	Mass rate of erosion per unit area.
E_c	Critical rate of erosion.
k	Number of predictors in a model.
M	Linear erosion rate constant.
n	Number of points in a dataset.
R^2	Coefficient of determination.
R^2_{adj}	Coefficient of determination adjustment for multiple predicting variables.
SE	Standard error.
SS_E	Sum of the squares of the unexplained deviations of the measured values from the model.
SS_R	Sum of the squares of the explained deviations of the predicted values from the measured mean.
SS_T	Total sum of the squares of the measured values.
τ	Applied shear stress at the bed.
τ_c	Critical shear stress of erosion.
τ_{*c}	Shields Parameter.
τ_{y1}	Lower yield stress as measured in the rheometer.

τ'_{y1}	Lower yield stress estimated at a water content of 150%.
τ_{y2}	Upper yield stress as measured in the rheometer.
τ'_{y2}	Upper yield yield stress estimated at a water content of 150%.
y, $\bar{y}$, and $\hat{y}$	Generic dependent variable, its mean, and its predicted values.

SUMMARY

Samples collected from 5 bridge sites from around the state of Georgia are analyzed to determine their erosion and rheologic behavior. Most sites were subject to large amounts of local scour due to flood events resulting from Tropical Storm Alberto in 1994. According to the Federal Highway Administration's Hydraulic Engineering Circular No. 18 by Richardson and Davis (2001), scouring of bridge foundations is the most common cause of bridge failure resulting from floods. The erosion rates of the soils are measured in a rectangular tilting flume capable of applying up to 21 Pa of shear stress at the bed. Samples from Shelby tubes are extruded into the flow from below the bed using a hydraulic piston. The displacement is measured as a function of time using a cable-pull potentiometer. The soils are also subject to extensive geotechnical analysis. Sieve and hydrometer analyses are performed to obtain the particle size distribution for each sample. Atterberg Limits and other standard geotechnical measures are also found. Additionally, insight into the shear strength and cohesive nature of the fine (<0.75 μm) particles is gained using a stress controlled rheometer to measure the rheological characteristics of the slurry. These results are used to improve and extend a relationship for the critical shear stress of soils developed in previous research that can be used in bridge scour prediction formulae as affected by soil parameters. In addition, the rheologic properties of the soil in terms of a dimensionless yield stress are related to the critical value of the Shields parameter for estimating critical shear stress for erosion.

CHAPTER I

INTRODUCTION

In an unaltered state, river systems reach a transient equilibrium as the natural hydrodynamic forces exerted by the flow on the river bed constantly erode and deposit alluvial sediments. This natural transport of sediments is what causes a river's path to widen and meander, and creates constantly evolving bed forms such as ripples, dunes, and sandbars. Unusually high stresses on a channel's bed caused by intense storm events, urbanization of the tributary watershed, and flow obstructions such as bridge piers or the contraction of abutments will disturb the natural evolution of a river and result in higher rates of erosion than deposition. This net loss of sediment, known as scour, is known to compromise the integrity of bridge foundations and have adverse impact on the river's ecology.

During high discharges, contractions at bridge abutments cause accelerations of the flow through the entire contracted section. Obstructions such as piers cause flow separation, resulting in vertical flow towards the river bed that forms a horseshoe vortex. The increased stress on the bed caused by these processes can be powerful enough to fluidize the bed at the piers and create scour holes at the foundation of a bridge. These processes, contraction and local scour, are the primary cause of failure of bridge foundations and other hydraulic structures (Richardson and Davis, 2001). Resisting the tendency to scour away sediments are two primary forces: the weight of the sediment particles and cohesive interparticle forces. The submerged weight of the particles is the dominant resistive force for what will later be defined as coarse particles. By contrast, fine sediments are so small that their submerged weight becomes negligible, and the

electrochemical forces determined by their mineralogy dominate the resistance to erosion.

In the Mid-Atlantic region of the US, 73 bridges were destroyed by flooding in 1985. Two years later in New York and New England, spring floods destroyed or damaged 17 bridges due to scour. Floods in 1993 caused 23 bridge failures and $15 million in damages to the upper Mississippi basin. In Georgia, Tropical Storm Alberto caused an estimated $130 million in damage to 500 state-owned bridges in 1994. In some cases, Alberto created scour holes as deep as 20 ft at bridge piers (Richardson and Davis, 2001).

It is the primary objective of this project to determine the erosion characteristics of sediments from five bridge foundations across the state of Georgia in a manner that continues and extends the work of Navarro (2004). Using Shelby tube samples of sediment cores, the erosion rate of the sediments are measured as a function of the bed shear stress. Quantities describing the erosion behavior of the sediments are then related to common geotechnical characteristics. A secondary goal is to determine the rheologic properties of slurry made of the fine particles of the sediments with the use of a stress controlled rheometer. A relationship between those properties and the geotechnical characteristics is also investigated.

In addition, an effort is made to relate the erosion characteristics from the flume tests to the more robust rheologic properties. Since the rheologic properties of a sediment can be determined with far less lab equipment, less sampling of the sediment, in shorter time spans, and in a manner less prone to operator error, bridge engineers and hydrologists would benefit greatly from being able to estimate the erosion rates near bridges from a few geotechnical and rheologic properties. For example, Brandimarte et al. (2006) studied the erosion properties of sediments near a pier of the Woodrow Wilson Bridge in Washington, DC. Stream flow data was then synthesized using a 68-year historical

flood record and stochastic modeling techniques. Employing a Monte Carlo simulation scheme, the resulting hydrographs were used in conjunction with the critical shear stress data of local sediments to predict a design scour depth for a proposed bridge south of the Woodrow Wilson Bridge. In a similar vein, this study seeks to advance the state of the practice of bridge foundation design with respect to characterizing the erosion characteristics of Georgia soils.

Chapter 2 of this report contains a literature review of recent publications on the behavior of river, estuarine, and marine sediments, various methods used to measure the erosion properties of soil, and the rheology of cohesive sediments. Chapter 3 details the experimental methods and materials used throughout the course of this project. The results of the laboratory work and analysis are presented in Chapter 4. Lastly, the conclusions, proposed modifications to the experimental procedures, and recommendations for future research are found in Chapter 5.

CHAPTER II

LITERATURE REVIEW

2.1 Sediment Characteristics

Particle size is a primary factor controlling the ability of a soil to resist erosion. Soil particles that are retained on the No. 200 (75 μm) sieve are classified as coarse. For these particles, body forces govern the erosion process. The weight force scales with the cube of the particle diameter, while the drag force scales with the square of the diameter. Material small enough to pass the No. 200 sieve is considerably more complex, however. Known simply as "fines" or as "silt and clay," these particles are subject to electrochemical forces that can depend on the pH of the porewater as well as the water and organic contents of the sediment (Ravisangar et al., 2001; Black, 2002; Krishnappan, 2007).

These forces become the most prevalent when the particle size shrinks down from silt to clay particles at roughly 2 μm. This is partially due to the fact silts are largely formed from mechanical weathering and therefore retain a spherical shape. Resulting from chemical weathering processes, clay particles have very large specific surface areas due their plate-like structures. Because of this change in particle behavior, the forces contributing to erosion resistance include van der Waals forces, Coulombian attraction, electrical double layer forces, and hydration forces in addition to the gravitational and buoyant forces that dominate the behavior of coarser materials (Mahmood et al., 2001).

2.1.1 Non-cohesive Sediments

Following Santamarina (2001) and Sturm (2001), below is a summary of the forces governing the erosion of non-cohesive silts and sands, assuming a spherical particle shape. The force of weight and buoyancy acting on a soil grain are as shown:

$$F_W = \frac{1}{6}\pi G_s \gamma_w d^3 \tag{2.1}$$

$$F_B = \frac{1}{6}\pi \gamma_w d^3 \tag{2.2}$$

with G_S as the specific gravity of the soil grain, γ_w the unit weight of water, and d the particle diameter. The difference between these two forces is known as the submerged weight.

$$W_s = F_W - F_B \tag{2.3}$$

Another force exerted on a soil grain at rest is the viscous drag force caused by the fluid flowing around it:

$$F_D = \frac{1}{2}\mathbb{C}_D \rho_w A_f u^2 \tag{2.4}$$

In Equation 2.4 above, $\mathbb{C}_D$ represents the drag coefficient, ρ_w the density of water, A_f the frontal area of the particle, and V is the flow velocity of the imparting fluid. Thus for non-cohesive sediments, erosion occurs when the drag force is larger than the submerged weight ($F_D > W_s$). For an open channel, the hydrodynamic force per unit area is known as the applied shear stress, τ. This is expressed as

$$\tau = \gamma_w R S \tag{2.5}$$

where R is the hydraulic radius (flow area divided by wetted perimeter) and S is the slope of the channel. Following Sturm (2001), the applied shear stress at which sediment motion is initiated is defined as the critical shear stress, τ_c,

$$\tau_c = f_1(\gamma_s - \gamma_w, d, \rho_w, \mu) \tag{2.6}$$

where $\gamma_s - \gamma_w$ is the submerged specific weight and μ is the dynamic viscosity of water. Through dimensional analysis of Equation 2.6, it follows that

$$\tau_{*c} = \frac{\tau_c}{(\gamma_s - \gamma_w)d} = f_2\left(\mathbf{Re}_{*c} = \frac{d\sqrt{\frac{\tau_c}{\rho_w}}}{\nu}\right) \tag{2.7}$$

where ν is the kinematic viscosity, and $\mathbf{Re}_{*c}$ and τ_{*c} are dimensionless and introduced as the critical boundary Reynolds number and the Shields Parameter, respectively. Shields (1936) developed these two parameters to describe incipient sediment motion in the widely used Shields diagram. The Shields parameter represents the ratio of the applied shear stress to gravitation force per unit volume. The critical boundary Reynolds number approximates the ratio of the particle diameter and the thckness of the viscous sublayer. The critical shear stress and particle diameter are both included in the definitions of the parameters, thus preventing a simple and direct relationship between the two sediment properties. A third dimensionless quantity,

$$\Pi = \sqrt{\frac{0.1\mathbf{Re}_{*c}^2}{\tau_{*c}}}$$

allows the critical shear stress to be directly determined from the particle diameter, resulting in the following form of the dimensionless particle diameter, d_* (Julien, 1995). This relationship assumes a uniform particle diameter for the sediment, When working with natural materials, the median particle size (d_{50}) is often used. The Shields Diagram relating τ_{*c} to d_* is shown in Figure 2.1.

$$\tau_{*c} = f_3\left(d_* = \sqrt[3]{\frac{(G_s - 1)\, g\, d^3}{\nu^2}}\right) \tag{2.8}$$

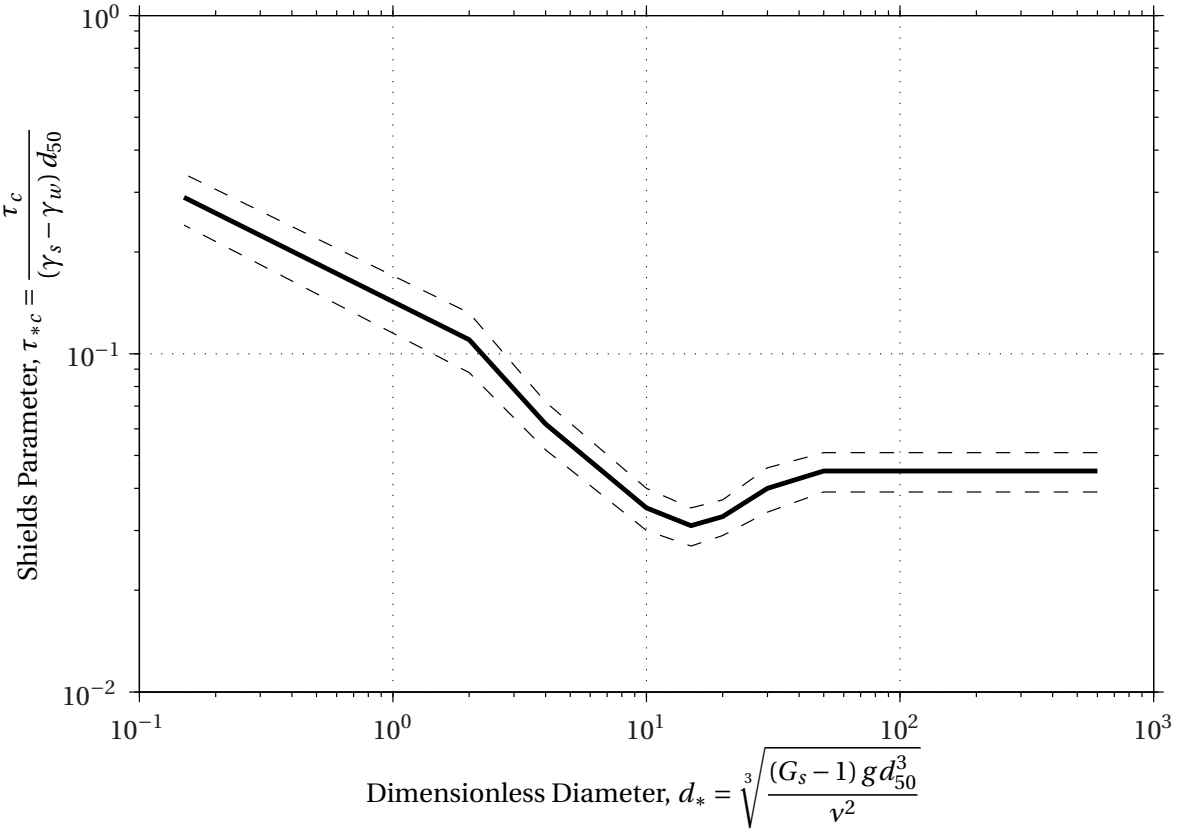

Figure 2.1: The Shields Diagram: τ_{*c} vs. d_* (Sturm, 2001)

2.1.2 Cohesive Sediments

Cohesive sediments are subject to several other forces in addition to gravity. These forces greatly depend on the chemistry of the sediment and the water, which determine the sediment structure.

Most structural configurations can be classified as one of the following: Edge-to-Face (E-F), Edge-to-Edge (E-E), Face-to-Face (F-F), or Shifted Face-to-Face (van Olphen, 1977). Combinations of these particle arrangements are illustrated in Table 2.1. Mahmood et al. (2001) summarized the equations for the hydration forces, electrical double layer forces, van der Waals forces, and Born repulsion forces associated with E-E, E-F, and F-F of kaolinite particles. Kaolinite particles are thin, hexagonal plates with negative ions on the broad faces and positive ions arranged on the thin edge. This results in substantial changes in particle behavior and arrangement due to changing pore water

Table 2.1: Particle associations in fine, cohesive sediments (van Olphen, 1977)

Clay Particles	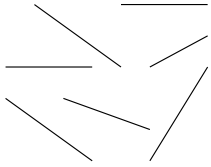	Dispersed, Defloculated	
Simple Particle Associations	E-F Flocculated, but Dispersed 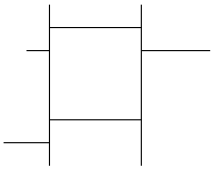	E-E Flocculated, but Dispersed 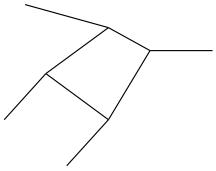	F-F Aggregated, but Dispersed 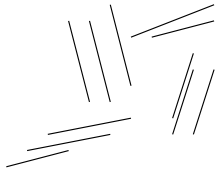
Mixture of Particle Associations	E-F Flocculated, F-F Aggregated 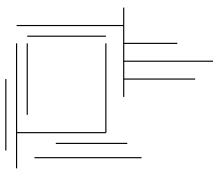	E-E Flocculated, F-F Aggregated 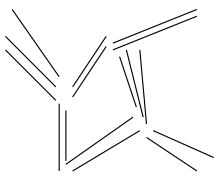	E-E, E-F Flocculated, F-F Aggregated 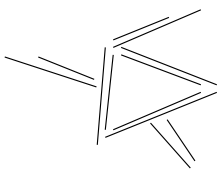

chemistry (e.g., pH, ionic strength, organic matter content) (Mahmood et al., 2001; Ravisangar et al., 2001, 2005; Krishnappan, 2007). The results of studies by Mahmood et al. (2001) and Ravisangar et al. (2001) show that the cohesion of kaolinite particles follows the sequence below.

$$F-F \gg E-F > E-E$$

The forces of E-F arrangements were found to be larger than E-E structures by a factor of $\sqrt{2}$. Maximum particle detachment occurs at a porewater pH of approximately 5, which corresponds largely to E-E configurations.

Later studies (Ravisangar et al., 2005; Gerbersdorf et al., 2006) delved further into the effect of pore water chemistry on cohesive sediment stability. Ravisangar et al. (2005) added natural organic matter (NOM) from water collected from Georgia's Suwannee River to commercially available kaolinite, which was allowed to settle over a 24-hour period. Erosional strength and bulk density both increased with depth in the settled sediment bed when the measured pH was less than 5.5. The structural arrangements of the bed changed as a function of the pH, organic matter content, and ionic strength. Lastly, it was found that the erosional strength was mostly a function of the bulk density when E-F and F-F arrangements predominate. Gerbersdorf et al. (2006) conducted similar experiments with natural sediments from the banks of the River Neckar in Germany. The critical shear stress and bulk density of the sediments were measured with depth. The presence of extracellular polymeric substances (EPS), or biofilms, dominated the measured vertical profiles, though there was weak correlation to the amount of biomass that produced the EPS in the sediment. Overall, it was concluded that the median particle size, total organic carbon, carbon exchange capacity, and EPS, affected the measured τ_c the most.

2.2 Modes of Erosion

Forms of erosion previously identified include surface erosion, mass erosion, and fluidization Partheniades (1965); Mehta (1991). During bed erosion, all three modes may be present in some proportion, though one typically dominates (Mehta, 1991).

Surface erosion and mass erosion were identified by (Partheniades, 1965). Surface erosion occurs when the applied shear stress is at or above the sediment's critical shear stress. Material is transported away from the bed as individual grains or small flocs (cohesive groups) of grains. The rate of surface erosion will increase with the applied shear stress. At what Partheniades (1965) identified as the macroscopic shear strength of the bed, the sediment can fail along an entire plane below the surface, transporting downstream all of the material above the failure plane. This phenomenon is known as mass erosion.

Fluidization, as defined by Mehta (1991), results when the eroding fluid penetrates into the pores of a sediment, thereby relieving the load of the skeletal forces and destroying the sediment structure. The sediment is subsequently entrained by the eroding fluid and mixed as downstream transport occurs.

2.3 Erosion Measurements and Relationships

Properties of soils and sediments that allow investigators to estimate their erosion characteristics can be measured in several ways both in the laboratory and the field. In either setting, the erosion flumes and impinging jets are both common apparatus.

2.3.1 Submerged Impinging Jets

Following Paterson (1989), Tolhurst et al. (1999) built, calibrated, and used what was called a cohesive strength meter (CSM) to measure the critical shear stress of estuarine sediments *in situ*. The device consisted of two concentric cylinders with a brass nozzle above the center. The CSM was carefully placed on the estuarine sediment to be tested and the area open to the sediment (6.6 cm^2) was filled with the local estuarine water. The submerged jet discharged in pulses applying up to 200 Pa of shear to the sediments. Optical sensors measured the light transmission through the water as the test progressed to determine when the sediment began to erode. The whole process was fully automated by an on-board computer. The device was initially calibrated using sieved quartz sands and reproduced values obtainable from the Shields diagram. The critical erosion pressure measured by the CSM exhibited a strong exponential relationship to the median grain size (d_{50}) of the sediment.

Mazurek et al. (2001) and Ansari et al. (2003) both used submerged circular jets to study the erodibility of soils in a laboratory. Both apparatus involve filling a large cylindrical tank with water and lowering a nozzle to a specified height above the sediment bed surface. Mazurek et al. (2001) measured only the erosion characteristics of clays with nozzle diameters ranging from 4 mm to 8 mm, and jet velocities between 4.97 m/s and 25.98 m/s. Maximum scour depth, scour depth at the jet centerline, and scour hole volume were measured at doubling time intervals until an equilibrium was reached. These values were primarily related to characteristics of the jet, rather than characteristics of the soil. Ansari et al. (2003) used artificial mixtures of clay and sand (d_{50} = 0.27 mm and 5.3 μm, respectively) with the sand portion ranging from 10% to 60% by mass. The nozzle diameter and height above the sediment varied between, 8.0 mm to 12.5 mm and 0.15 m to 0.3 m, respectively, with jet velocities ranging from 1.3 m/s to 5.75 m/s. The depth and side slopes of the hole and the rate of scour were measured and empirically related

to the clay content, dry density, and water content of the soils prior to testing.

While studying the managed realignment of embankments of intertidal salt marshes in Essex, UK, Watts et al. (2003) used vertical impinging jets to study the local clayey marine alluvium *in situ*. Bulk properties were also tested. Most notably the undrained shear strength was measured with a Geonor fall-cone penetrometer. A high correlation between the undrained shear strength and critical shear stress as measured with the CSM was found. Shugar et al. (2007) used a very similar device to measure the erodibility of soil *in situ*. A large steel tank is pounded into the banks of a tributary stream of the Credit River near Toronto, Canada. Water from the creek is used to fill the tank and subsequently is impinged on the ground surface. The depth of the scour hole formed is measured every two minutes. The erodibility of the natural soil was the focus of the investigation and thus the results were not related to any of its characteristics.

2.3.2 Laboratory Flumes

Laboratory flumes are also commonly used to study the erosion characteristic of soils and sediments. McNeil et al. (1996) eroded rectangular sediment cores from rivers in a straight rectangular flume. The cores were 100 mm wide and 150 mm long and were placed at the end of the 1.35 m long flume. Applied shear stresses ranged from 0.2 Pa to 10 Pa and the vertical erosion rate ($\dot{z}$) was measured visually with a meter ruler. The critical shear stress was defined as the applied shear stress where 10^{-3} mm/s $< \dot{z} <$ 10^{-2} mm/s. Dry and wet bulk densities, water content, grain size distributions, and total organic carbon of the samples were measured, but could not be related to the critical shear stress. Fluid characteristics, such as pH however, could be related to the critical shear stress in a manner similar to Ravisangar et al. (2001). Zreik et al. (1998) allowed Boston Blue Clay to deposit from suspension in an annular flume 0.5 m in diameter and rectangular cross sectional dimensions of 0.3 m by 0.3 m. By rotating the floor and lid of

the flume in opposite directions, bed shear stresses ranging from 0.1 Pa to 1 Pa were applied to the sediment bed. Surface erosion was observed in all cases where the applied bed shear stress was slowly and incrementally increased. The one case where the test was initially brought up to maximum shear exhibited mass erosion-like characteristics. Zreik et al. (1998) concluded that thixotropic hardening occurs as the settle sediments age, the shear stress history has little effect on the erodibility of the sediment, and that most of the Boston Blue Clay's resistance to erosion was provided by the bonds between sediment flocs and increased with depth. Additionally the mechanical strengths of the sediment were measured with an apparatus similar to a traditional fall-cone device and were found to be one order of magnitude larger than the erosional strength. Krishnappan (2007) used a flume 4.72 m in diameter to measure the size distribution of sediment flocs and the settling behavior at low applied shear stresses.

What is now known as the Scour Rate in Cohesive Soils-Erosion Function Apparatus (SRICOS-EFA) was developed by Briaud et al. (1999) and later refined by Briaud et al. (2001). The EFA consists of a rectangular acrylic duct with a bottom port for extruding standard Shelby tube (76.2 mm diameter) samples into the flow for erosion. Bed shear stresses ranging from 0.1 Pa to 100 Pa are measured by two pressure ports immediately upstream and downstream of the sample as it is continuously extruded to maintain a steady height of 1 mm above the flume bed. Initial tests showed that samples extrusion heights of approximately 2 mm would produce significantly larger erosion rates than what would occur at heights between 0 mm and 1 mm; thus the 1 mm height was chosen. The SRICOS procedure also specifies that the sample be submerged one hour prior to testing and dictates an increasing sequence of flow velocities to maintain until 1 mm of sample erodes or one hour passes, whichever is first. SRICOS-EFA allowed the investigators to measure erosion rates as low as 1 mm/day and as high as several meters per hour. During these two studies, the erosion rates of silts and clays exhibited no significant correlation to geotechnical characteristics such as undrained shear strength,

percent passing the No. 200 (75 μm) sieve, and plasticity index.

The SRICOS procedure (but not an EFA) was used by Ting et al. (2001) to measure the scour depth of silts and clays around piers 25 mm and 75 mm in diameter. The piers and sediments were placed in a variable-slope, rectangular flume 27.30 m long, 0.46 m wide, and 1.22 m deep. Initial bed bathymetry and flow characteristics were measured with an acoustic Doppler velocimeter (ADV) and point gauge mounted to an instrument carriage on top of the flume. The shape of the scour hole was found to be related to the pier Reynolds number. At low pier Reynolds numbers, the scour hole was evenly distributed around the pier. Higher pier Reynolds numbers produced larger holes primarily behind the pier. The clays eroded very slowly and the results were fitted to hyperbolic curves. Equilibrium scour depths predicted by the fit were found to be consistent with the guidance in HEC-18. Both equilibrium scour depths predicted by Ting et al. (2001) and HEC-18 correlated well with the pier Reynolds number. Sediments for the River Neckar in Germany were studied by Dey and Westrich (2003). Rectangular cores were placed at the end of a glass flume 8 m long, 0.25 m wide, and 0.60 m deep. An ADV was used to measure progress of the scour hole formed at the transition from the glass bottom of the flume to the sediment core. The average critical shear stress of the material was found to be 2.5 Pa and had a median particle size of 17 μm. Witt and Westrich (2003) used an experimental apparatus based on that of McNeil et al. (1996). The sediment cores eroded were 135 mm in diameter, and the flume had a 7.8 m approach section, was 0.15 m wide, and 0.1 m deep. Witt and Westrich (2003) also used a traditional rectangular flume, but used a unique approach to measure erosion. Thirty laser lines were continuously projected onto the sediment surface as it eroded. To measure the volume eroded with time, computer-based image analysis compared photographs collected every 3 seconds to a baseline image captured prior to testing.

Roberts et al. (2003) used a rectangular (50 mm tall, 105 mm wide), enclosed flume to

measure the erosion rate, suspended and bedload transport, and total eroded mass of quartz particles with median particle sizes (d_{50}) of 19, 475, and 1250 μm and sediments from the Boston Harbor (d_{50} = 37.5 μm). The sediments were premixed, poured, and consolidated in the flume prior to testing. Samples were manually kept flush with the flume bottom and total mass eroded was measured by collecting and drying sediment particles settled into sediment traps. Barry et al. (2006) measured the effect of adding small amount of clay to sands by eroding well mixed beds in a rectangular flume 4.3 m long, 0.15 m wide, and 0.19 m tall. The last 0.6 m of the flume contained the sediment. Adding 0% to 15% (by mass) clay to the sediment caused strong lubrication influences and significantly reduced the critical shear stress.

Ganaoui et al. (2007) tested two cores of surface river sediments and a core of coastal sediment from 160 m below the sea bed. In a recirculating PVC flume 3.6 m long, the resuspension of the sediment was measured via turbidity, which was in turn related to the suspended sediment load measured by filtering grab samples of the water every 3 minutes. The samples were classified based on the magnitudes of the critical shear stresses. The first class of samples was identified as recently deposited "fluff" and were easily eroded. The second class of samples came from the deeper, more consolidated sediments. Class 2 sediments agreed well with past research, though the coarser samples deviate slightly from the Shields Diagram.

2.3.3 Benthic Flumes

Benthic flumes are essentially upside down channels placed on the bottom of a river, lake, harbor, or any other body of water where the erosion of sediments is of concern. Water is pumped through the flume so that the erosion and sediment transport can be measured in numerous ways. The major advantage of benthic flumes is that the flow

conditions (shear stress) of importance can be created on completely undisturbed sediments *in situ*. Ravens and Gschwend (1999) used a laser Doppler anemometer to measure the turbidity of the water pulled through a rectangular acrylic flume measuring 2.5 m long, 0.12 m wide, and 0.06 m tall. The flume was gently placed on the sediment bed where legs extended away from the flume and into the bed to stabilize the flume. Using a pump, water was pulled though the flume up to the boat where the turbidity was measured and later related to the erosion of the sediment. The entrance of the flume contained a 2.5 cm tall bar to trip a turbulent boundary layer as the applied shear stress ramped up in 10-minute intervals up to 30 Pa. The measured critical shear stress values agreed with the Shields diagram and could best be related to the depth of the sediment.

Aberle et al. (2003, 2004, 2006) used the National Institute of Water and Atmospheric Research *in situ* flume (NIWA I) to measure the erosion characteristics of natural sediment beds. The straight, rectangular flume measured 1.2 m long, 0.2 m wide, and 0.1 m tall with the last 0.9 m of the flume's length leaving the sediment bed exposed to the flume. A propeller driven by an electrical motor pulled water through the flume, eroding the bed. Turbidity was monitored at 1 Hz and averaged over a span of 30 seconds. Similar to Ravens and Gschwend (1999), data at each applied shear stress showed an initial spike in erosion that decayed exponentially. This behavior was attributed to depth-limiting properties of the sediments. Before the start of the tests, ambient conditions were recorded and five sediment samples from around the flume were collected to measure the wet and dry bulk densities, water content, loss on ignition (LOI) and grain size distribution of the sediments. Debnath et al. (2007a,b) used a second flume (NIWA II) that included modifications proposed in Aberle et al. (2004). The flume measured 0.74 m long, 0.16 m wide, and 0.08 m tall with a 0.6 m test section at the end. It contained turbidity meters near the entrance and exit of the flume and well as a current meter. It also employed an air pump to replace the electrical pump, reducing the electrical noise of the system. The NIWA II flume provided results very much comparable to NIWA I.

Recently, Ravens (2007) compared laboratory (McNeil et al., 1996) and *in situ* erosion measurements (Ravens and Gschwend, 1999) from the Lower Fox River in Wisconsin. Both samples were collected at the same site and similar depths. Quadratic models in the form of $E = M\tau^2$ were fit to the data to facilitate the comparison. It was shown that the samples tested in the laboratory were 5 times more erodible than the sediments tested *in situ*. It is proposed that the reasons behind this discrepancy is that the benthic flume has a 110 cm test section, which is significantly longer than the 15 cm section of the laboratory flume. This would exaggerate the differing effects of the transition from hard to soft beds present in both flumes. Additionally, some reviewers propose that the 5 year time span between testing events allowed more resistant sediments to migrate to the site. However, this claim is not supported by the associated geotechnical data and no biological mats were present during the *in situ* test.

2.4 Mathematical Models of Erosion

Mehta (1991) developed a simple and now widespread equation to describe erosion. The equation involved the mass rate of erosion per unit area, or erosion rate (E), and the difference between the applied bed shear stress (τ) and critical shear stress (τ_c) normalized by the critical shear stress, or excess shear stress. Over the course of this study, these two quantities are linearly related as shown in Equation 2.9,

$$E = M\left(\frac{\tau - \tau_c}{\tau_c}\right) \tag{2.9}$$

where M is a constant. The only ambiguity exists in the definition of the critical shear stress. In the past these definitions have included the shear stress at which erosion ceases or at which a predetermined small value of erosion occurs. Additionally, a linear regression can be performed on erosion rate and bed shear stress data. The shear stress corresponding to zero erosion on the best-fit line is yet another possible definition of τ_c. With any of the methods listed above, M and τ_c are uniquely determined by

the sediment and the fluid conditions present.

Equation 2.9 is by far the most commonly used, but other researchers have proposed relationships that include sediment properties. For instance, Roberts et al. (1998) developed Equation 2.10, which uses the bulk density of the sediment:

$$E = A\,\tau^n\,\rho_b^m \tag{2.10}$$

where A, n, and m are sediment-dependent constants. Quadratic equations have also been suggested.

$$E = b_0 + b_1\,\tau + b_2\,\tau^2 \tag{2.11}$$

In Equation 2.11, b_0, b_1, and b_2 are experimental constants (Donat, 1929).

The results of Roberts et al. (1998) and Zreik et al. (1998) were reviewed by Krone (1999). A piece-wise linear relationship was found to exist between the erosion rate and bulk density. The breakpoint occurs at a critical bulk density that causes the sediment structure to collapse due to the overburden.

Lee et al. (1994a,b) summarized τ_c values previously found from various researchers. Results ranged from 0.01 Pa for a loam with 19% fines up to 61 Pa for a soil with d_{50} = 5 μm. Similarly, Mehta (1994) reviewed data collected from numerous previous investigations. The vast collection of data was summarized with the following equation:

$$\tau_c = a_0 d + \frac{b_0}{d} \tag{2.12}$$

where d is the average particle diameter, and the constants a_0 and b_0 are empirical parameters. Continuing this work, Lick et al. (2004) developed the relationship below:

$$\tau_c = \left(1 + \frac{c_4}{c_3\,d^2}\right) 0.414 \times 10^3\,d \tag{2.13}$$

where

$$c_3 = \frac{\pi}{6}\left(\rho_s - \rho_w\right) g\,d^3 \tag{2.14}$$

and c_4 is determined with the sequence of equations below.

$$c_4 = c_4^* \frac{\tau_c(\rho, d_1)}{\tau_c^*} \tag{2.15}$$

$$\tau_c(\rho, d_1) = a_1 e^{b_1 \rho} \tag{2.16}$$

with $\tau_c^* = \tau_c(\rho_1, d_1) = 1.35$ N/m^2; $\rho_1 = 1.85$ kg/L; $d_1 = 5$ µm; and $c_4^* = 1.33 \times 10^{-4}$ N/m^2. Dong (2007) built upon Equation 2.17 proposed by Brownlie (1981) to calculate the Shields parameter for bimodal sediments:

$$\tau_{*c} = 0.22\mathbf{Re}_p^{-0.6} + 0.06 \times 10^{-7.7\mathbf{Re}_p^{-0.4}} = f(\mathbf{Re}_p) \tag{2.17}$$

with the particle Reynolds number, $\mathbf{Re}_p = \frac{d\sqrt{Rgd}}{\nu}$; $R = \frac{\rho_s - \rho_w}{\rho_w}$; d = particle size; ν is the kinematic viscosity of water. After reviewing the data published by Torfs (1995) and Panagiotopoulos et al. (1997), Dong (2007) developed the following equation for the ratio of the critical shear stress of the sand alone, to that of the silt/sand mixture:

$$\frac{\tau_{csf}}{\tau_{cs}} = \frac{f(\mathbf{Re}_m)}{f(\mathbf{Re}_s)} \tag{2.18}$$

where the $\mathbf{Re}_m$ and $\mathbf{Re}_s$ are the particle Reynolds numbers of the silt/sand mixture and sand alone, respectively. Mehta (1991) also summarized erosion relationships developed by several previous investigators. They are included in Table 2.2.

Table 2.2: Erosion rate expressions for cohesive sediment beds (Mehta, 1991)

Investigator(s)	Expression
Partheniades (1965)	$E = \alpha_1 \left[1 - \frac{1}{\sqrt{2\pi}} \int_{\frac{-\beta_1}{\tau-\beta_2}}^{\frac{\beta_1}{\tau-\beta_2}} \exp\left(\frac{-\omega^2}{2}\right) d\omega \right]$
Christensen (1965)	$E = \alpha_2 \left[0.5 - \frac{1}{\sqrt{2\pi}} \int_0^{-6.1+\frac{6.18}{\sqrt{\beta_3 \tau}}} \exp\left(\frac{-\omega^2}{2}\right) d\omega \right]$
Kandiah (1974); Arulandan (1975)	$E = \alpha_3 \left(\frac{\tau - \tau_c}{\tau_c} \right)$
Christensen and Das (1973); Raudkivi and Hutchinson (1974); Gularte (1978)	$E = \beta_4 \, e^{\alpha_4 (\tau - \tau_c)}$
Laberton and Lebon (1977)	$E = \alpha_5 \left(\tau^{\beta_s} - \tau_c^{\beta_s} \right) \tau^{1/2}$
Thorn and Parsons(1980)	$E = \alpha_6(z) \left[\tau - \tau_c(z) \right]$
Parchure and Mehta (1985)	$E = \alpha_7 \exp\left[\alpha_8 \sqrt{\frac{\tau - \tau_c(z)}{\tau_c(z)}} \right]$
Maa and Mehta (1987)	$E = \alpha_9 \left(\frac{\tau - \tau_r}{\tau_r} \right)$

2.5 Rheology Principles

The science describing the behavior of fluids influenced by applied shear stresses is known as rheology. Newtonian fluids are defined as fluids that deform under an infinitesimal applied shear stress and whose shearing rates will increase linearly with the applied shear stress. This can be modeled simply as a line with an intercept at zero and a slope equal to the viscosity of the fluid (Laird, 1957; Markovitz, 1985; Nguyen and Boger, 1992).

Hyperconcentrations of sediments do not follow this model and as such are considered

non-Newtonian. Up to a given shear stress, often refered to as the yield stress (τ_y), deformations in the fluid are elastic and recoverable when the shear stress is no longer applied. When the shear stress exceeds the yield stress, the deformation is permanent as the material starts to flow (Markovitz, 1985; Federico, 1999). In the simplest case, known as the Bingham plastic model, the viscosity of the fluid is constant after it yields (Laird, 1957; Nguyen and Boger, 1992). Thus both fluids can be modeled with the following equation:

$$\tau = \tau_y + \eta\,\dot{\gamma} \tag{2.19}$$

where τ is the shear stress, η is the viscosity, and $\dot{\gamma}$ is the strain rate. In the case of the Newtonian fluid, the yield stress is simply equal to zero. In addition to Bingham plastic behavior, what is known as shear-thickening and shear-thinning behaviors can occur. A non-Newtonian fluid exhibiting shear-thickening behavior will have a viscosity that increases with the strain rate. These fluids are said to be yield dilatant. Conversely, shear-thinning fluids decrease in viscosity with increasing shear stress and are said to be yield pseudo-plastic. Per Nguyen and Boger (1992), both of these characteristics can be modeled with an empirical exponential equation similar to Equation 2.19.

$$\tau = \tau_y + k\,\dot{\gamma}^m \tag{2.20}$$

In Equation 2.20, k and m are exponential parameters that model the varying behavior of the viscosities. A fluid is yield dilatant for $m > 1$ and yield pseudo-plastic for $m < 1$. It is also quite clear from Equation 2.19 and Equation 2.20 that Newtonian fluids and Bingham plastics are special cases described by this equation when $m = 1$ and $k = \eta$. Figure 2.2 illustrates how the types of fluids behave relative to one another (Nguyen and Boger, 1992). Flow curves are typically measured with a rheometer. Two primary types exist: strain controlled and stress controlled rheometers. The devices involve submerging and rotating a vane or probe in a fluid. Strain controlled rheometers are programmed

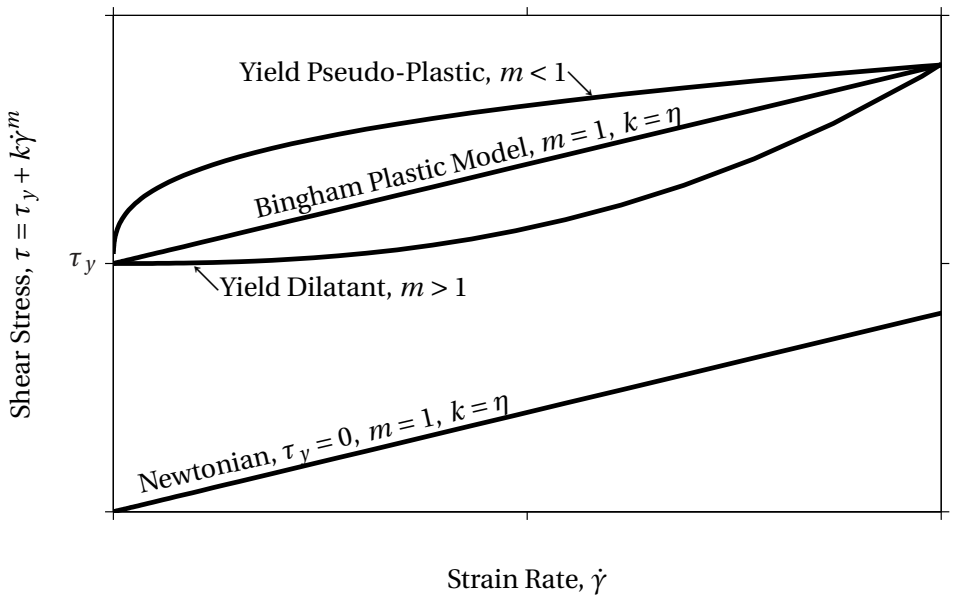

Figure 2.2: Theoretical flow curves of Newtonian and non-Newtonian fluids

to rotate at certain rates or amounts and measure the stress required to do so. Stress controlled rheometers programmatically apply shear stresses to the fluid and measure the resulting strain.

2.6 Rheology Studies

Previous research has sought to relate rheological parameters to the response of sediments to hydrodynamic forces. Before sediment particles can be resuspended and eroded, the bed must yield, irreversibly deforming as it flows. Wright and Krone (1987), Otsubo and Muraoka (1988), O'Brien and Julien (1988), Julien and Lan (1991) and van Kessel (1998) attempted to describe the transport of fine sediments using rheological parameters.

Both Wright and Krone (1987) and Otsubo and Muraoka (1988) directly used flume erosion and rheometer tests to characterize the erosional strength of fine sediments. Wright and Krone (1987) found the critical sediment concentrations at which sediments transitioned from exhibiting Newtonian to non-Newtonian behavior. It was determined that

at low concentrations, the sediment particles are unable to form sufficiently cohesive bonds and exhibit similar rheology over a great range of concentrations. Above the critical concentration, the particle interactions cause the yield stress and stress-strain relationship of the sediments to behave in a manner strongly dependent on the sediment concentration. Otsubo and Muraoka (1988) defined two critical shear stresses – one at onset of flume erosion and one at mass failure of the sediment bed – and related them to the yield stresses obtained with a rheometer. The two yield stresses defined by Otsubo and Muraoka (1988) are discussed further in Section 3.4.5.

Julien and Lan (1991) sought to build upon the basic rheologic model of sediment hyperconcentrations proposed by Bagnold (1954), in which friction and collisions amongst the particles explained shear stress under appreciable strain rates. It was found that particle cohesion, viscous interactions between particles and the fluid, and turbulence should also be considered. As a result, a dimensionless, quadratic model applicable to both Newtonian and non-Newtonian sediments is shown in Equation 2.21:

$$\tau = \tau_y + \eta\left(\frac{du}{dy}\right) + \zeta\left(\frac{du}{dy}\right)^2 \tag{2.21}$$

where ζ is a turbulent-dispersive parameter and $\frac{du}{dy}$ is the velocity gradient.

O'Brien and Julien (1988) measured the yield stress of the fine portions of natural samples collected in the Rocky Mountains of Colorado. Tests were conducted at various volumetric concentrations of sediment with capillary, cylindrical, and cone-plate viscometers. The cylindrical viscometer test produced the most reliable results for non-Newtonian fluids at a wide range of shear stresses, while the cone-plate configuration was more applicable in lower ranges of shear stresses. Sand was added to sediments and was found to have little effect below volumetric concentrations of 20% in the silt-clay mixtures. Sand concentrations larger than 20% were found to significantly increase the measured viscosity.

In a similar fashion, van Kessel (1998) measured the flow curves of several natural and artificial muds with stress controlled and strain controlled viscometers using a cone-plate configuration. Using the strain controlled devices, a variety of tests were performed. They included preshearing the sample at 100 s^{-1} and decreasing the strain rate down to a value dependent on the response of the material. Experiments were also performed where the torque required to harmonically oscillate the bob was measured. Lastly a strain controlled viscometer was used to measure the flow curves and yield stress recovery of sediments. It was found that flow curves are heavily influenced by the sediment's stress history at strain rates less than 5 s^{-1}. Additionally, yield stresses were best measured with the stress controlled viscometers.

CHAPTER III

EXPERIMENTAL MATERIALS AND METHODS

3.1 Sample Characteristics

The samples tested through the course of this project were collected by the Georgia Department of Transportation (GDOT) in accordance with ASTM D 1578-00: "Standard Practice for Thin-Walled Tube Sampling for Geotechnical Purposes." The steel tubes, known as Shelby tubes and shown in Figure 3.1, have an outer diameter of 76.2 mm (3 in.), length of 910 mm (36 in.) and wall thickness of 1.65 mm (0.065 in.). The drilling crews were given the bridge foundation depths and the most convenient drilling and sampler insertion methods were chosen based on the specific conditions of each site. Once received, the samples were stored vertically in a constant-temperature room. Flume tests were performed on the samples to find the critical shear stress of the ma-

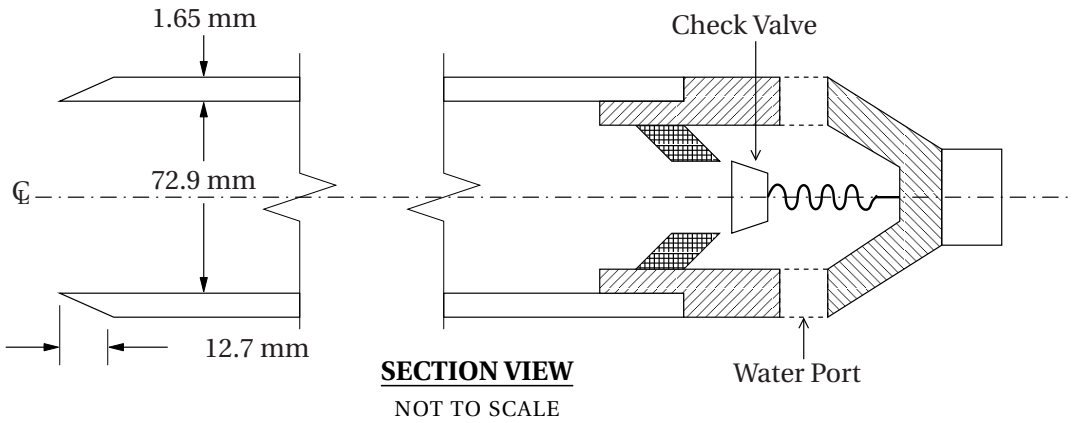

Figure 3.1: Undisturbed 3-inch thin walled sampler

terial. Extensive geotechnical analyses were also carried out to further characterize the soil based on properties such as grain size distribution, bulk densities, Atterberg limits,

and organic matter content. Samples were collected throughout the state of Georgia at bridge sites selected to complement the previous work of Navarro (2004) in a way that provides broader coverage of Georgia's physiographic regions.

Georgia has seven main physiographic regions. Figure 3.2 illustrates the location of each collection site and the physiographic regions. Sample locations indicated by dark circles and numbered 11 through 15 were the focus of this study while the other locations were investigated by Navarro (2004). Figure 3.3 similarly shows the sample locations relative to Georgia's major land resource areas (MLRAs). Table 3.1 summarizes each sample location and physiographic region.

Table 3.1: Sample locations and physiographic regions

No.	County	Location	Physiographic Region	Major Land Resource Area	Latitude & Longitude
11	Meriwether	SR 362 over Red Creek	Southern Piedmont	Southern Piedmont	33.172 °N, 84.506 °W
12	Monroe	SR 42 over Towaliga River	Southern Piedmont	Southern Piedmont	33.372 °N, 84.232 °W
13	Houston	US 341 over Bay Creek	Sea Island & Eastern Gulf Coastal Plain	Southern Coastal Plain	32.475 °N, 83.776 °W
14	Stewart	CR 99 over Holchodkee Creek	Sea Island & Eastern Gulf Coastal Plain	Sand Hill	32.036 °N, 84.782 °W
15	Candler	SR 23 over Canoochee River	Sea Island	Southern Coastal Plain	32.190 °N, 81.956 °W

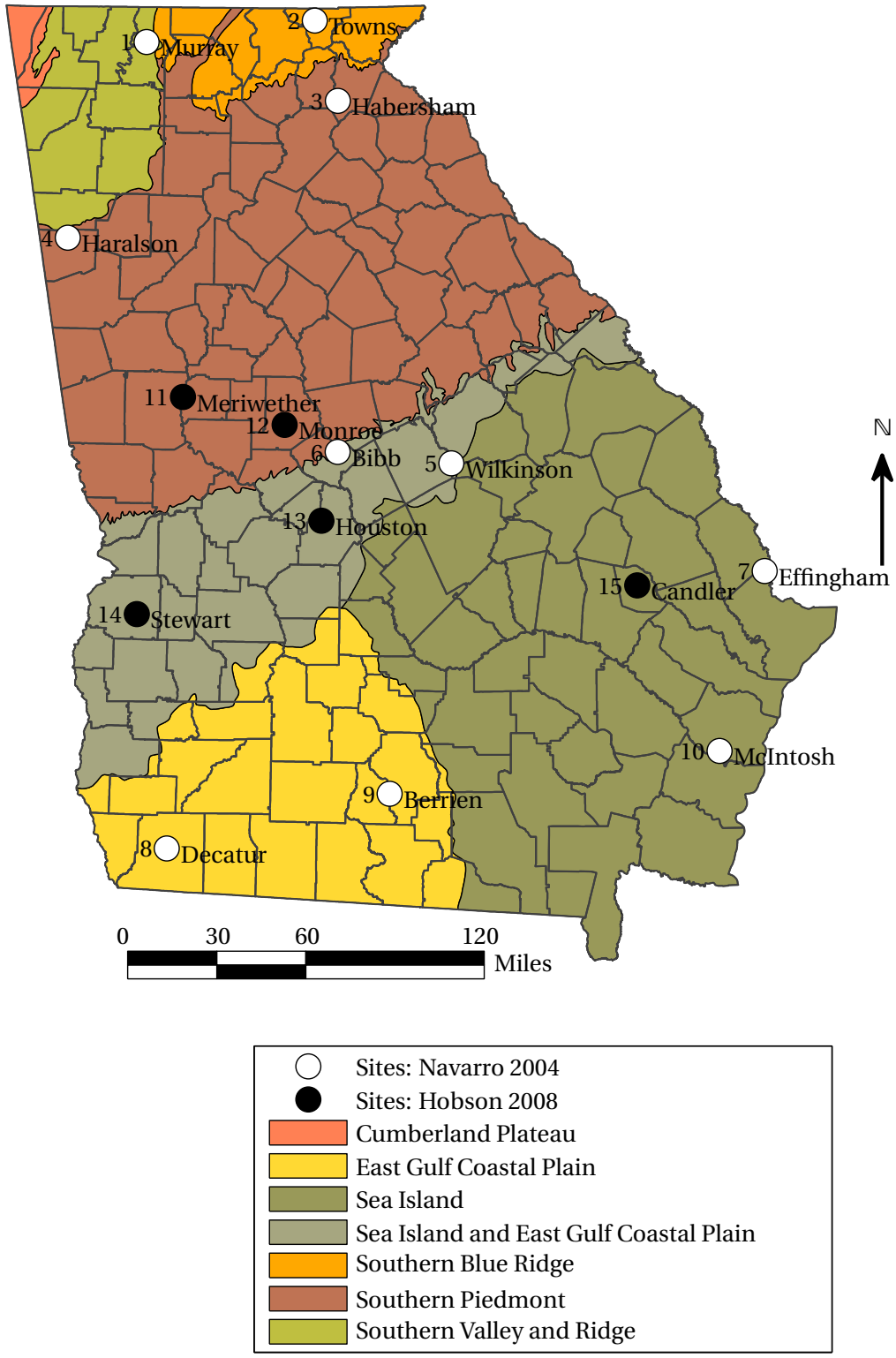

Figure 3.2: Previous and current sample locations and Georgia physiography (Alhadeff et al., 2000)

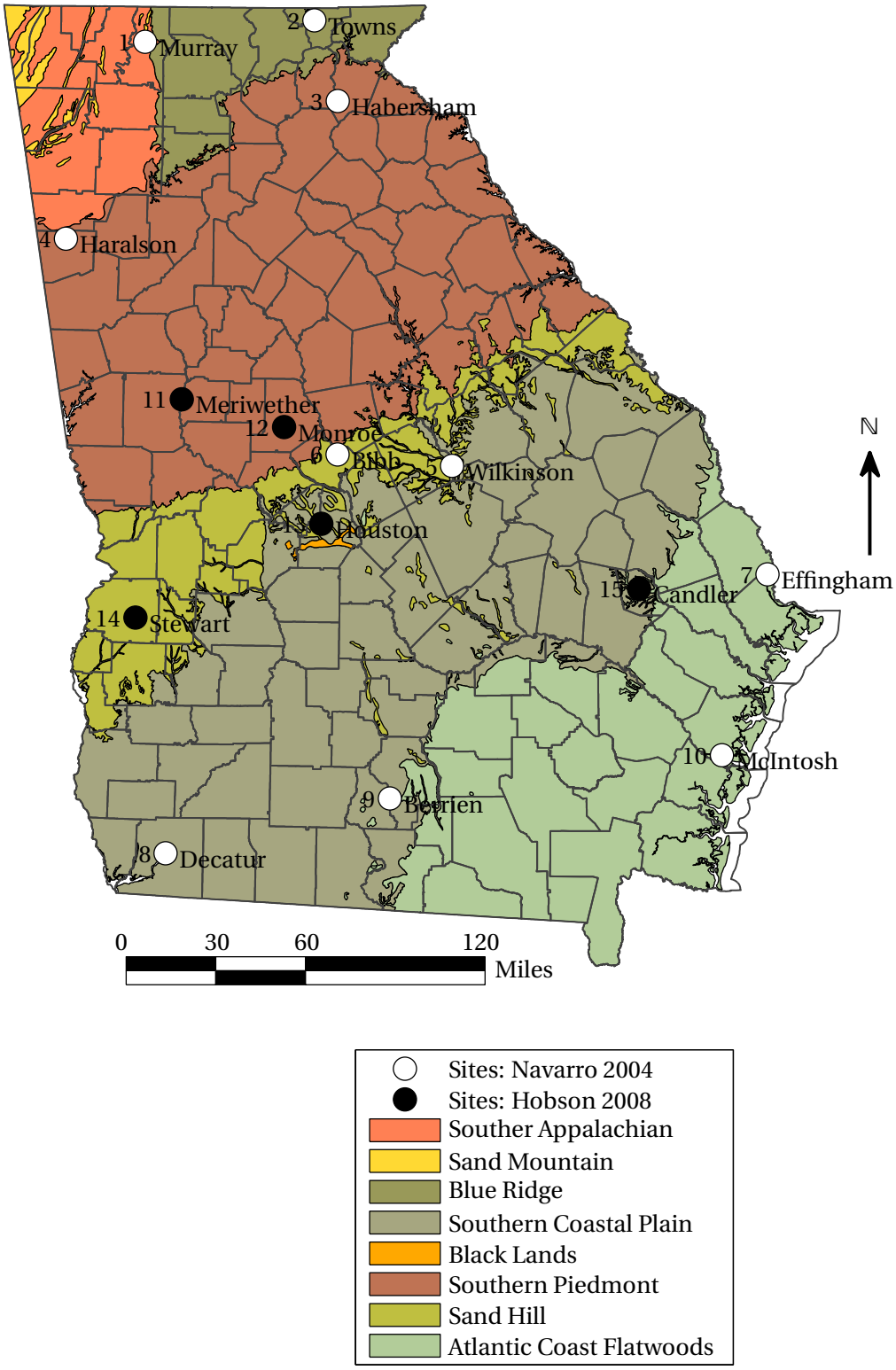

Figure 3.3: Previous and current sample locations and Georgia major land resource areas (Alhadeff et al., 2000)

3.2 Experimental Setup

The samples were eroded in a recirculating, rectangular, tilting flume located in the Hydraulics Laboratory at the Georgia Institute of Technology. The flume measures 6.1 m long, 0.38 m wide, and has a maximum depth of 0.38 m (20 ft × 1.25 ft × 1.25 ft). The flume has a fixed gravel bed (d_{50} = 3.3 mm), which ensures that the flow encountered by the sample is fully-developed and fully-rough turbulent flow as $\mathbf{Re}_{*c} = \frac{u_{*c}\, d_{50}}{\nu}$ ranges from approximately 70 to 500 for τ_c = 0.4 to 21 Pa. The flume is fed from a 1.9 m^3 storage tank by one variable speed, large-impeller centrifugal pump designed for solids pumping. An illustration of this system is shown in Figure 3.4. To produce the desired shear stress in the flume, the discharge, depth of flow, and bed slope are controlled by the operator. The discharge is controlled by the rotation speed of the pump in use. Previous researchers developed the flow calibration of a bend meter shown in Figure 3.5 (Ravisangar et al., 2001; Hoepner, 2000). The pump is capable of producing discharges between 14.2 L/s to 70.8 L/s (0.5 ft^3/sec to 2.5 ft^3/sec). The bend meter was calibrated by measuring the discharge with a weigh tank for small discharges and a magnetic flow meter for larger discharges. The discharge was then correlated with manometer deflection measured from the bend meter. The uncertainty of the calibration is 0.0057 ft^3/sec. The tilting flume can be set to slopes ranging from 0 (horizontal) to 0.02 m/m. Steeper slopes are mechanically possible with the flume, but due to the highly supercritical flow ($\mathbf{Fr} > 1$), achieving a stable flow regime becomes quite difficult. The slope is measured with a mechanical counter that counts the rotations of the gear that raises and lowers the downstream end of the flume. Figure 3.6 shows the calibration of the slope counter. The depth of flow is controlled either by the flume's tailgate for subcritical flows or by the upstream sluice gate during experimental runs with supercritical flows. Normal depth was calculated from the asymptotic approach depth of gradually-varied flows during preliminary experiments. Using the normal depth guarantees uniform flow and allows

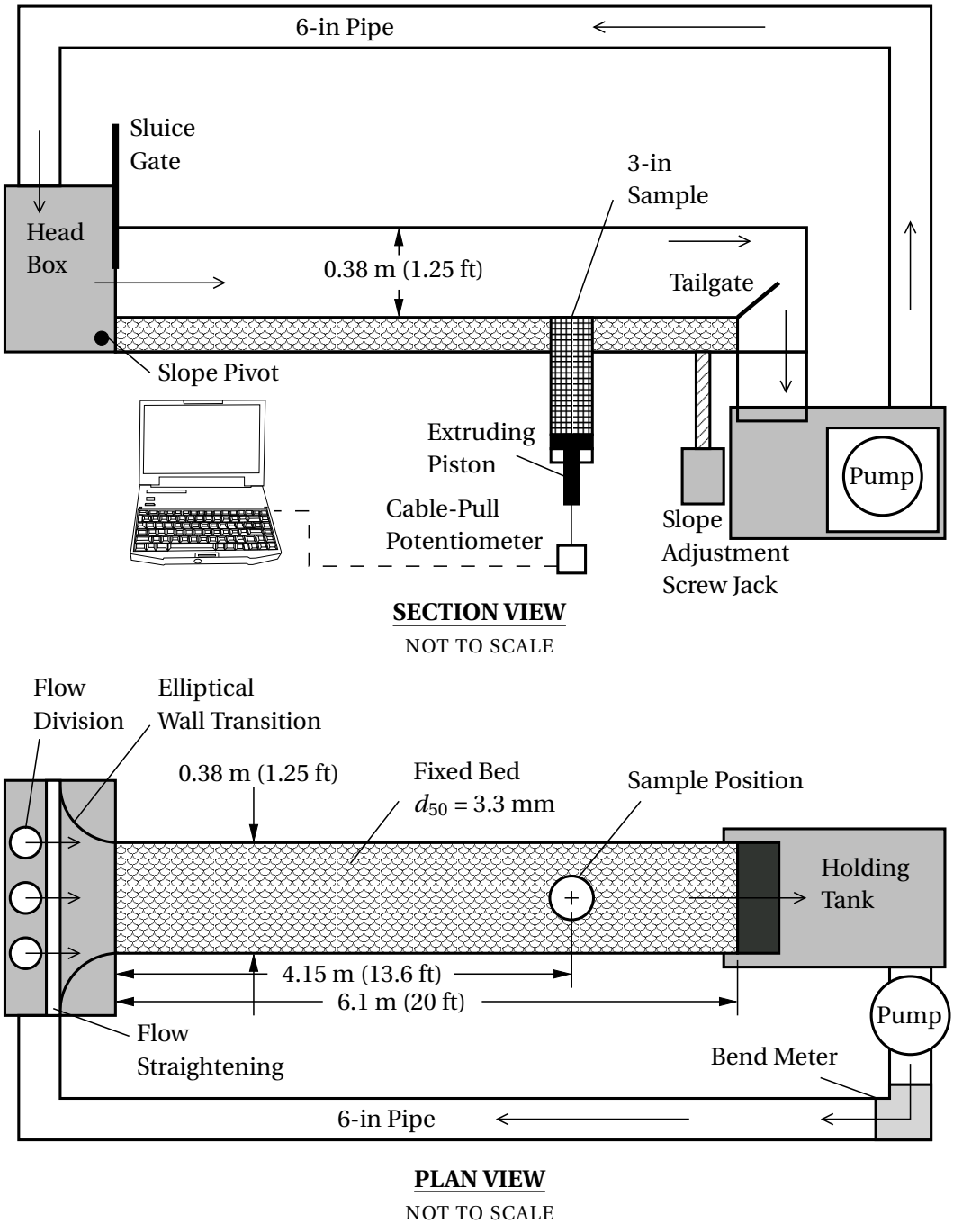

Figure 3.4: Tilting, recirculating flume for erosion testing

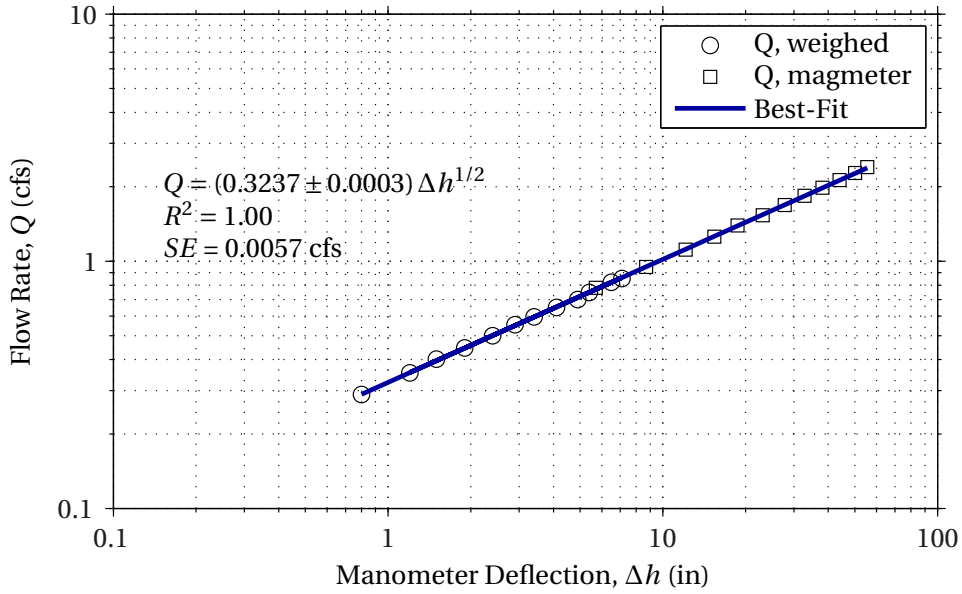

Figure 3.5: Pump bend meter calibration

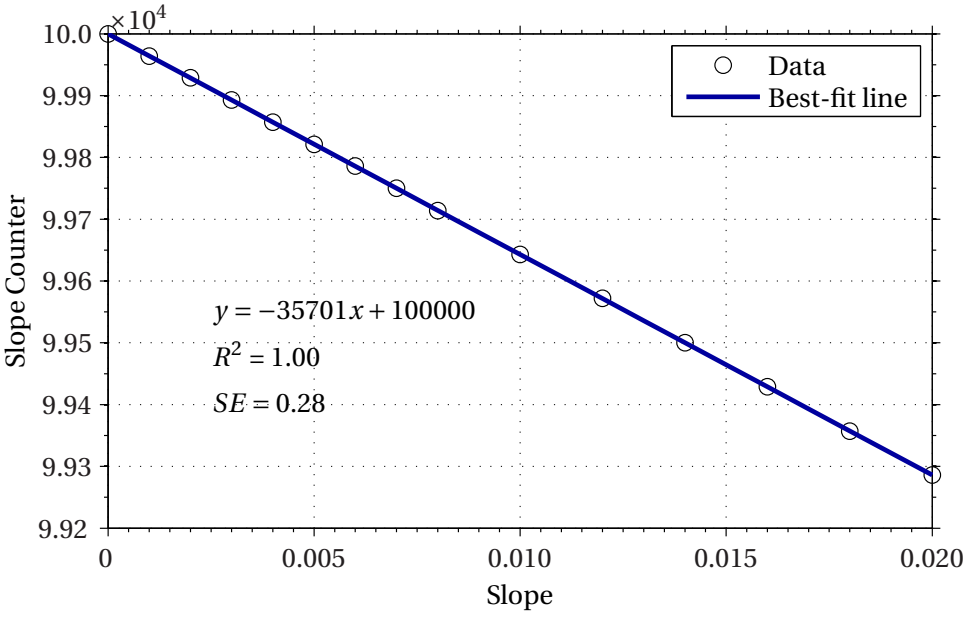

Figure 3.6: Calibration of the flume slope counter

the bed shear stress to be determined from the uniform flow equation. Ravisangar et al. (2001) measured the velocity profile in the flume with a laser Doppler velocimeter (LDV). From the slope of the centerline velocity profiles fitted by a logarithmic distribution, the bed shear stress was calculated. The results confirmed that the shear stress applied to the bed at the sample (τ) can be calculated as the product of the water specific weight (γ_w), the flow depth (y), and the channel slope (S), for a given flow regime, as given by Equation 3.1.

$$\tau = \gamma_w \, y \, S \tag{3.1}$$

The bed shear stress applied to the samples ranged from 0.4 Pa to 21 Pa. The flow depths used in the flume ranged 0.04 m to 0.2 m. The approximate maximum average velocity is 1.7 m/s. The boundary Reynolds number ranged from 70 to 500 during the experiments, well into the range of fully-rough, turbulent flow (Sturm, 2001).

At the start of each experiment, uniform flow depths were set using the tailgate or sluice gate based on the inital measurement of normal depth and the roughness coefficient for the combinations of flow rate and slope. In order to maintain accurate uniform flow depths, the Froude (**Fr**) number was kept below 2 to prevent roll waves. A correction was applied to the roughness factor to account for the smooth (acrylic) sidewalls and rough bed at different Reynolds numbers (**Re**). For a rectangular sectioned flume, the Froude number is given by

$$\mathbf{Fr} = \frac{V}{\sqrt{g\,y}} \tag{3.2}$$

where V is the mean flow velocity and g is gravitational acceleration. Additionally, the Reynolds number (**Re**) and friction factor (f) are defined as

$$\mathbf{Re} = \frac{4\,R\,V}{\nu} \tag{3.3}$$

$$f = \frac{8\,\gamma_w\,R\,S}{\rho_w\,V^2} \tag{3.4}$$

in which ν is the kinematic viscosity of the water; γ_w is the specific weight of the water; S

is the bed slope; R is the hydraulic radius; and ρ_w density of the water. The hydraulic radius is the quotient of the flow area and wetted perimeter. In the case of the rectangular flume used in the experiments

$$R = \frac{b\,y}{b + 2\,y} \tag{3.5}$$

where b is the width of the flume.

A sidewall correction procedure prescribed by Julien (1995) was used to determine wall friction factor (f_w); bed friction factor (f_b); bed hydraulic radius (R_b); and Manning's roughness coefficient (n_b) as determined from the bed friction factor.

$$f_w = 0.0015\left[\log\left(\frac{\mathbf{Re}}{f}\right)\right]^2 - 0.0428\log\left(\frac{\mathbf{Re}}{f}\right) + 0.1884 \tag{3.6}$$

$$f_b = f + \frac{2y}{b}\,(f - f_w) \tag{3.7}$$

The hydraulic radius is then corrected with the bed friction factor from Eq. 3.4 to give the bed hydraulic radius:

$$R_b = \frac{f_b}{f}\,R \tag{3.8}$$

Then using the relationship between Manning's n and the friction factor f, the Manning's roughness coefficient for the bed can be found:

$$n_b = \frac{1.49}{\sqrt{8g}}\,R_b^{1/6}\,f_b^{1/2} \tag{3.9}$$

The equivalent sand grain roughness of the bed was determined by Ravisangar et al. (2001) through a nonlinear regression of Keulegan's equation:

$$\frac{n_b}{k_s^{1/6}} = \frac{\dfrac{K_n}{(8g)^{1/2}}\left(\dfrac{R_b}{k_s}\right)^{1/6}}{2.0\log\left(12.2\dfrac{R_b}{K_s}\right)} \tag{3.10}$$

The known quantities are n_b and R_b. The value of k_s is selected to produce the best fit of Eq. 3.10 to the experimental data. The resulting value of the equivalent sand-grain roughness is:

$k_s = 5.52$ mm $\pm$ 0.025 mm (0.0181 ft $\pm$ 0.00083 ft).

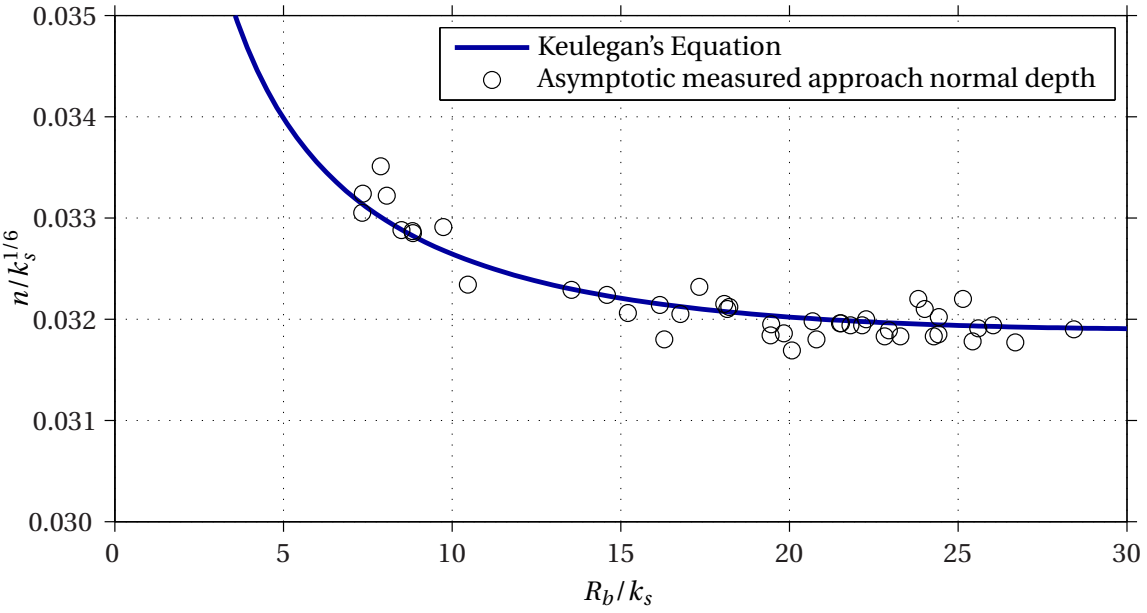

Figure 3.7: Measured and calculated bed roughness at various shear stress conditions

The best-fit value is approximately 5/3 times median grain size (d_{50}). Figure 3.7 shows a plot of $n_b/k_s^{1/6}$ against R_b/k_s. This is used to determine the normal depth at a shear stress range of 13 Pa to 21 Pa using Manning's equation and should follow the same fit of Keulegan's equation. Past flume experiments corroborated the normal depth predictions. After the Shelby tube has been inserted into the flume for testing, the erosion of the sample is measured with a cable-pull potentiometer. The potentiometer cable is attached to the hydraulic piston that extrudes the sample into the flume. The voltage output is read through a LabView virtual interface. Figure 3.8 shows the piston displacement-voltage relationship found during the calibration.

3.3 Erosion Rate and Critical Shear Stress

The following sections describe the experimental and mathematical procedures used to determine the erosion characteristics. The mathematics used to determine the erosion rate and critical shear stress of a sample follow that of Navarro (2004).

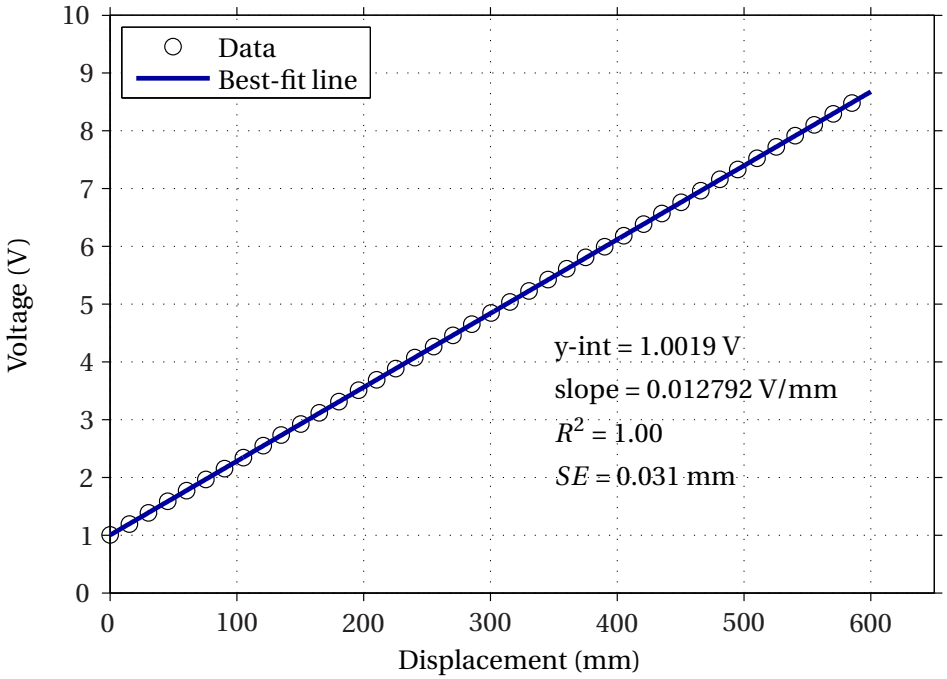

Figure 3.8: Potentiometer calibration to determine piston displacement

3.3.1 Measuring Critical Shear Stress and Erosion Rate

Throughout the testing in the titling flume, measureable erosion fell into two modes previously defined by Mehta (1991). Pure surface erosion is defined as single particles being eroded uniformly over the entire sample surface. Conversely, sometimes samples erode in the mode known as mass erosion. Mass erosion occurs when the entire section fails along a weak plane, transporting downstream all the material above. The existence of the two modes is not mutually exclusive, though they are related to the amount of fines (percent silt plus clay) and the excess shear stress relative to the critical shear stress.

Once the Shelby tube sample has been placed inside the flume and extruded to 1 mm above the fixed gravel bed, the exposed sample is shielded with a large metal plate and the flow is started. Ideally, the flow conditions are set such that the flow applies a shear stress at or slightly above the sample's critical shear stress.

The entire experiment relies on visual observation of the sample surface exposed to the

flow. As the sample erodes, the operator must use the piston to further extrude the sample such that the sample surface maintains a consistent height just above the fixed gravel bed. The upward movement of the piston as the sample is eroded and extruded is measured with the cable-pull potentiometer. Figure 3.9 shows a potentiometer data record collected during the testing of the sample from Monroe County collected at 5 ft to 7 ft below ground surface (BGS) under an applied bed shear stress of 6.40 Pa (0.134 lb/ft^2). After a sample has eroded anywhere from approximately 40 mm to 120 mm, the metal

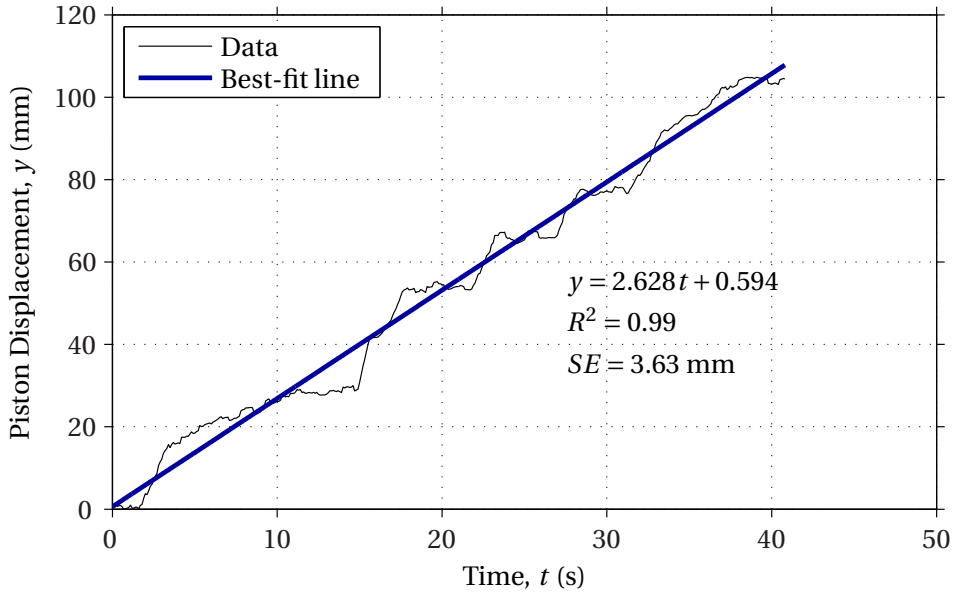

Figure 3.9: Example flume erosion measurement of Monroe County 5 ft to 7 ft BGS with an applied bed shear stress of $\tau = 6.40$ Pa

plate is again placed on top of the sample and the flow conditions are changed to apply a larger bed shear stress. At some point between tests, the flow is stopped so that approximately 500 g of material can be extruded for geotechnical characterization. If the material contains a significant portion of fines, an additional 200 g to 300 g are extruded for rheological testing. The flow then resumes at a new shear stress. The testing continues as long as possible or until the material or erosion rate changes drastically, at which point the flow must be shut down and the process of determining the critical shear stress restarted. At times, enough material would be suspended in flow to impede

visual observation of the sample. The flume would be entirely shut down, drained, and then restarted with fresh water. Using some measured geotechnical quantities of the samples described in Section 3.4, the erosion rate in mass of soil per unit time eroded during a test is calculated in the following manner:

$$\text{Erosion Rate} = E = \frac{\Delta y}{\Delta t}\,\rho_{dry} \tag{3.11}$$

where $\Delta y/\Delta t$ is the best-fit slope of the piston displacement data as shown in Figure 3.9 and ρ_{dry} is the dry density (i.e., dry mass per unit volume), of the material eroded.

3.3.2 Calculating Critical Shear Stress and Erosion Rate Constants

The critical shear stress of the soils tested is by far the most important parameter to be defined during this study. In order to determine this value, the erosion rate of the soil must be measured at several bed shear stresses, some which ideally will be near some minimum erosion rate. Similar to McNeil et al. (1996), the tilting flume used in this study can measure erosion rates as low as 0.001 kg/m^2/s.

Two basic models are used to fit the erosion rate vs. applied shear stress data. The first is a linear model:

$$E = M\left(\frac{\tau - \tau_c}{\tau_c}\right) \tag{3.12}$$

and the second is an exponential model.

$$E = E_c\, e^{a\left(\frac{\tau - \tau_c}{\tau_c}\right)} \tag{3.13}$$

The variables M and a are the erosion rate constants. Both models use the excess shear stress $(\tau - \tau_c)$ as the independent variable. For the linear model, the critical shear stress is determined by extrapolating the straight line to an erosion rate of zero. Due to the asymptotic nature of the exponential model, the critical shear stress is defined as the point where the curve reaches a negligible amount of erosion. Previous investigators

defined this value as E_c = 0.00190 kg/m^2/s (Navarro, 2004). This critical erosion rate value was determined while calibrating the erosion apparatus using a commercial sand with d_{50} = 1.16 mm. Both linear and exponential models resulted in a critical shear stress within the Shields range (Navarro, 2004).

Navarro (2004) compared the data to Karim's sediment transport equation (Equation 3.14). There was excellent agreement at lower shear stresses, with appreciable deviations at high shear stress. This is likely due to the fact that Karim's model predicts bedforms at the higher shear stresses, which is an impossible phenomenon to reproduce given the fixed bed in the flume (Sturm, 2001).

$$\frac{q_t}{\sqrt{(G_s-1)\,g\,d_{50}^3}} = 0.00139\left(\frac{V}{\sqrt{(G_s-1)\,g\,d_{50}}}\right)^{2.97}\left(\frac{u_*}{w_f}\right)^{1.47} \tag{3.14}$$

3.4 Soil Characteristics Testing

All samples were characterized by conventional geotechnical tests with material recovered directly from the Shelby tube. Additional material was recovered when there was a significant change in the erodibility or appearance of the material during an experimental run. Soil is a natural material, thus heterogeneity was expected and found in nearly all samples. The geotechnical tests included the following: dry and bulk densities, water content, specific gravity of soil grains, organic matter content, Atterberg Limits, and grain size analysis by sieve and hydrometer. Rheologic analyses were also performed to measure the lower and upper yield stresses of the fines of the soil in a stress controlled rheometer.

3.4.1 Bulk and Dry Densities

The bulk density of the material was estimated by extruding a small portion of the material from the Shelby tube and determining its mass. The length of the sample was measured with the potentiometer during extrusion. The diameter was determined by averaging several measurements of the inner diameter of the Shelby tube. The bulk density was calculated as

$$\rho_b = \frac{M_{sw}}{V_t} \tag{3.15}$$

where M_{sw} is the mass of the wet soil and V_t is the volume of the sample as calculated from the measured length and diameter of the extrusion. A portion of the sample was dried in an oven at 100 °C to a constant mass to determine the *in situ* water content (Equation 3.17), which was used to determine the dry mass of the soil grains (M_s). The dry density was determined with Equation 3.16.

$$\rho_d = \frac{M_s}{V_t} \tag{3.16}$$

3.4.2 Water and Organic Matter Content

Water content of the material was determined in accordance with ASTM D 2216-05: "Standard Test Methods for Laboratory Determination of Water (Moisture) Content of Soil and Rock by Mass." The document defines the water content as follows:

$$w = \frac{M_{pws} - M_{ps}}{M_{ps} - M_p} = \frac{M_w}{M_s} \tag{3.17}$$

where the subscripts p, w, and s indicate quantities relating to the the pan, pore-water, and soil grains, respectively.

The organic matter content of the soils was determined in a furnace capable of 500 °C (932 °F) provided by an environmental engineering laboratory in the School of Civil and Environmental Engineering at Georgia Tech. Tests were carried out per ASTM D 2974-00:

"Standard Test Method for Moisture, Ash, and Organic Matter of Peat and other Organic Soils." The organic matter content is defined as:

$$OM = \frac{M_s - M_{ash}}{M_s} \tag{3.18}$$

in which M_s is the mass of the soil dried to a constant mass at 100 °C (212 °F) and M_{ash} is the mass of soil after reaching a constant mass at 440 °C (824 °F)

3.4.3 Specific Gravity, Void Ratio, and Porosity

The specific gravity of the soils grains was determined by the method outlined in ASTM D 854-00: "Standard Test Method for Measuring Specific Gravity of Soil Solids by Water Pycnometer." The document details the necessary materials and apparatus to find the specific gravity of the soil grains by

$$G_s = \frac{M_s}{M_{\varrho w} - (M_{\varrho ws} - M_s)} = \frac{\rho_s}{\rho_w} \tag{3.19}$$

where the subscript ϱ refers to the pycnometer, while ρ_s and ρ_w are the densities of the soil grains and water, respectively. From this equation, it follows that $\rho_s = G_s \rho_w$. The ratio of the volume of the voids (i.e., air and water) of a soil to the volume of soil grains, or void ratio (e), can then be defined as shown in Equation 3.20

$$e = \frac{V_t - V_s}{V_s} = \frac{\rho_s}{\rho_d} - 1 \tag{3.20}$$

With a known void ratio, the porosity, n, of the soil can then be determined.

$$n = \frac{e}{1+e} \tag{3.21}$$

3.4.4 Atterberg Limits and Grain Size Distribution

Atterberg limits, namely the plastic limit (w_{PL}) and liquid limit (w_{LL}), provide some insight into the basic nature (e.g., clay content, consistency) of a fine-grained soil. The

plasticity index (I_p) is defined as the difference between the liquid limit and plastic limit. The guidelines for determining these parameters are found in ASTM D 4318-00: “Standard Test Method for Liquid Limit and Plasticity Index of Soils,” while the liquid limits of soils were found using a fall cone apparatus. The fall cone test is popular among engineers and scientists outside the US and is regarded as a better practice since its results are more repeatable and operator independent (Budhu, 2000). The standard procedure of the fall cone test is outlined in British Standard 1377-1990: “Method of Tests for Soils for Civil Engineering Purposes.” Figure 3.10 compares these two methods. Figure 3.11

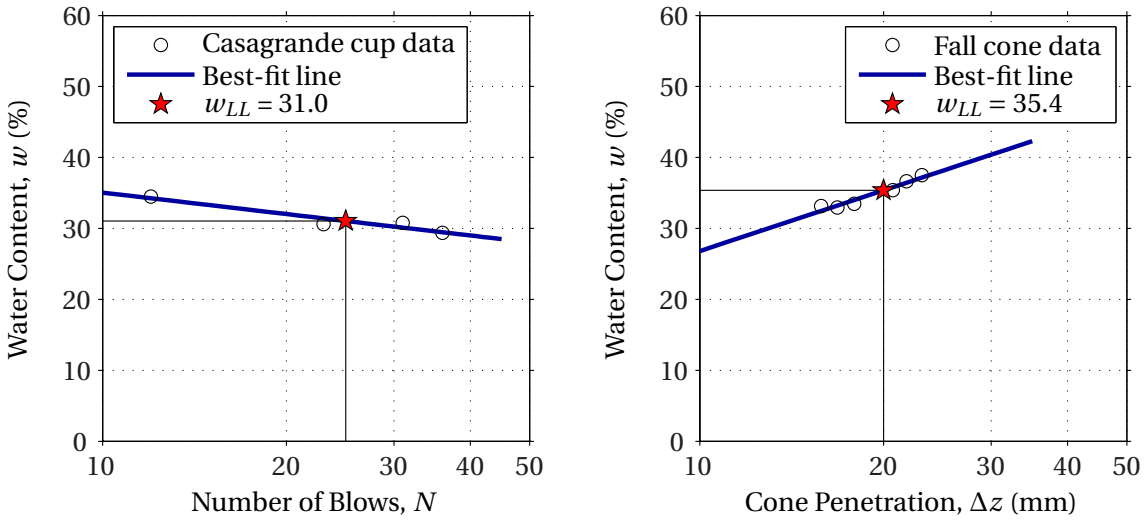

(a) Casagrande cup apparatus (b) Fall cone apparatus

Figure 3.10: Liquid limit test data using (a) Casagrande cup and (b) fall cone apparatus

shows the soil plasticity chart along with the results for all of the samples.

Sieve and hydrometer analyses were used to determine the grain-size distribution of the soils. Tests were carried out in accordance with ASTM C 136-01: “Standard Test Method for Sieve Analysis of Fine and Coarse Aggregate," and ASTM D 422-63 (Reapproved 2002): “Standard Test Method for Particle-Size Analysis of Soils," respectively. Figure 3.12 shows typical size distributions of selected samples. In a qualitative sense, the particle diameters of the clay minerals can lead to conclusions regarding the mineralogy of clay as

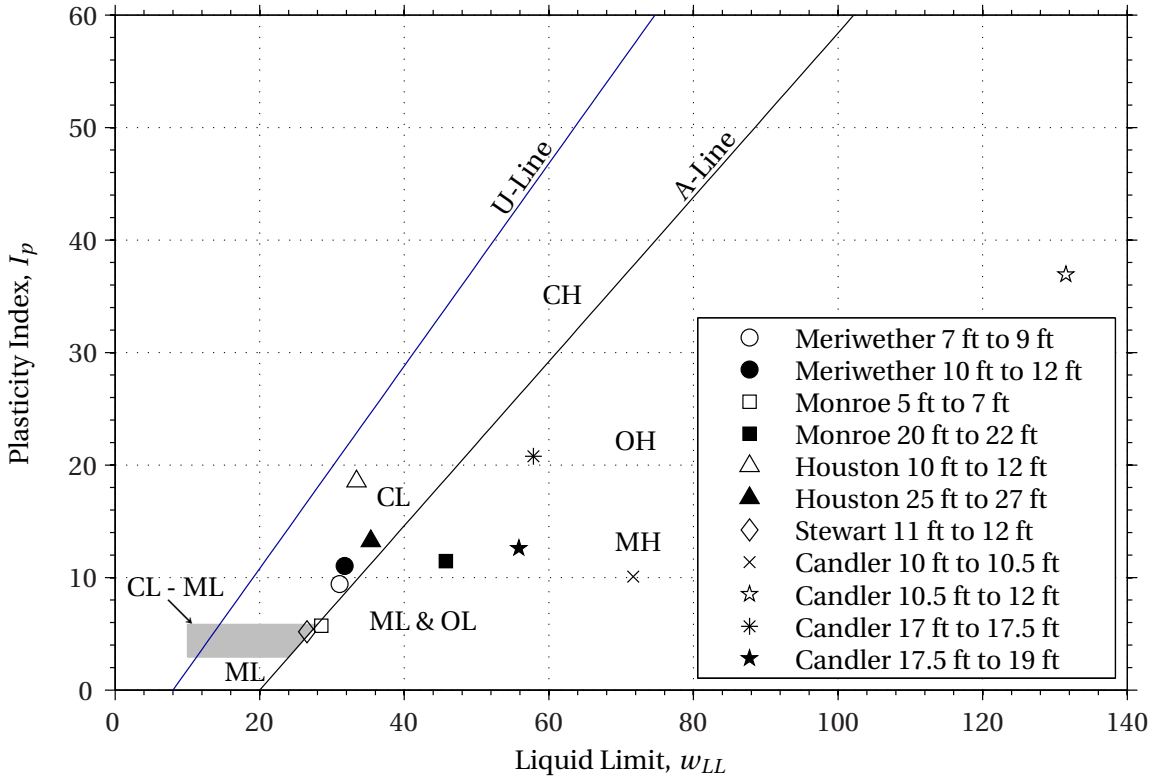

Figure 3.11: Soil plasticity chart

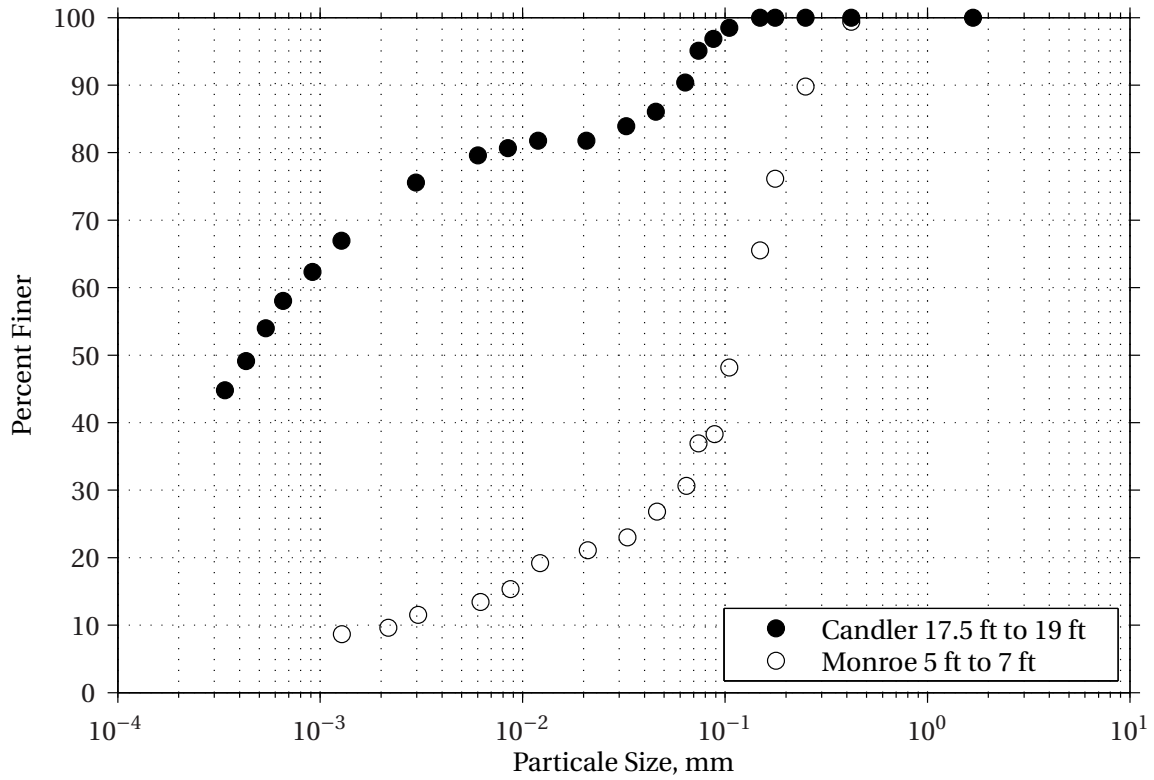

Figure 3.12: Typical grain-size distribution chart showing two samples

show in Table 3.2 from Mitchell and Soga (2005). The activity of a soil (I_A) is calculated

Table 3.2: Mineral composition of grain size ranges in soil (Mitchell and Soga, 2005)

Particle Size (μm)	Predominating Constituents	Common Constituents	Rare Constituents
0.1	Montmorillonite	Mica intermediates	Illite
0.1–0.2	Mica intermediates	Kaolinite, Montmorillonite	Illite, Quartz
0.2–2.0	Kaolinite	Illite, Mica intermediates	Quartz, Montmorillonite
2.0–11.0	Mica, Illites	Quartz, Kaolinite	Montmorillonite

as the quotient of the plasticity index and the clay content by mass (% finer than 2 μm) of a soil as shown in Equation 3.22. This provides qualitative insight into the mineralogy of the fine fractions of sediments. Following Fell et al. (2005) and Mitchell and Soga (2005), Table 3.3 summarizes the liquid limits, plastic limits, and activities of various clay minerals.

$$I_A = \frac{I_p}{clay} \tag{3.22}$$

Table 3.3: Atterberg Limits and activity of common clay minerals (Fell et al., 2005; Mitchell and Soga, 2005)

Mineral	Liquid Limit	Plastic Limit	Activity
Montmorillonite	100–900	50–100	1–7
Illite	60–120	35–60	0.5–1.3
Kaolinite	30–110	25–40	0.3–0.5
Mica and Calcite	–	–	0.2
Quartz	–	–	0

3.4.5 Yield Stress Analysis

The yield stress experiments were performed with a Haake RheoStress RS65 stress controlled rheometer provided by an environmental engineering laboratory in the School of Civil and Environmental Engineering at Georgia Tech. A rheometer is a device designed to measure the viscosity of a fluid as a function of the applied shear stress. The instrument basically consists of a cup and a concentric cylinder that is submerged then driven to rotate in the fluid. The test is used to as a means of directly estimating the strength of the cohesive bonds of the fines of a sediment. Only the fines can be used to prevent significant damage to the cup and cone of the rheometer. Figure 3.13 shows the experimental setup. Details of the cup and cone of the rheometer are found in Figure 3.14.

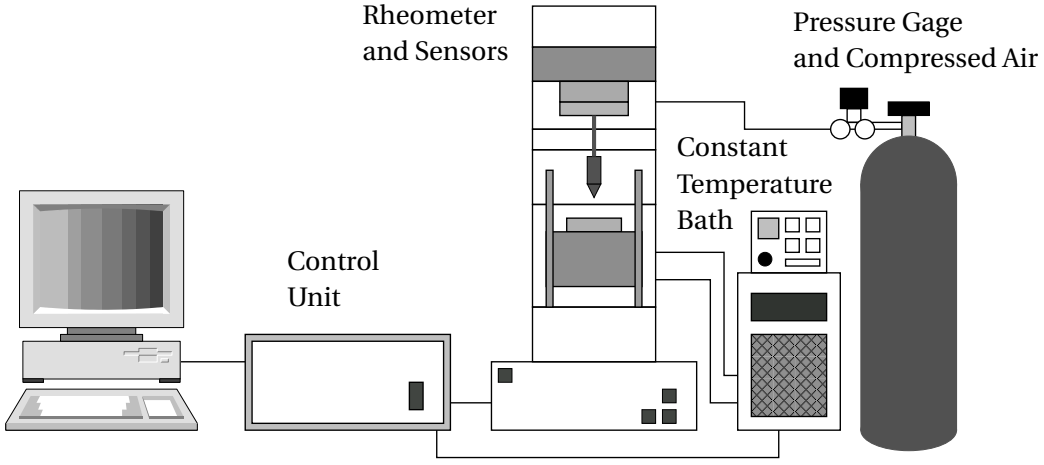

Figure 3.13: Stress controlled rheometer apparatus

After the geotechnical analysis of a sample was completed, any remaining sample material was washed over the No. 200 (75 μm) sieve with deionized water to fully segregate the fine from the coarse material. All of the wash water was retained and then oven dried in a silicon baking dish to prevent any particles from permanently attaching to its sides. The dry fine particles of the sample were recovered and stored in sealed containers until the yield stress analysis was to take place. Prior to the analysis, portions of the dry sample were restored to three to five increasing water contents with deionized

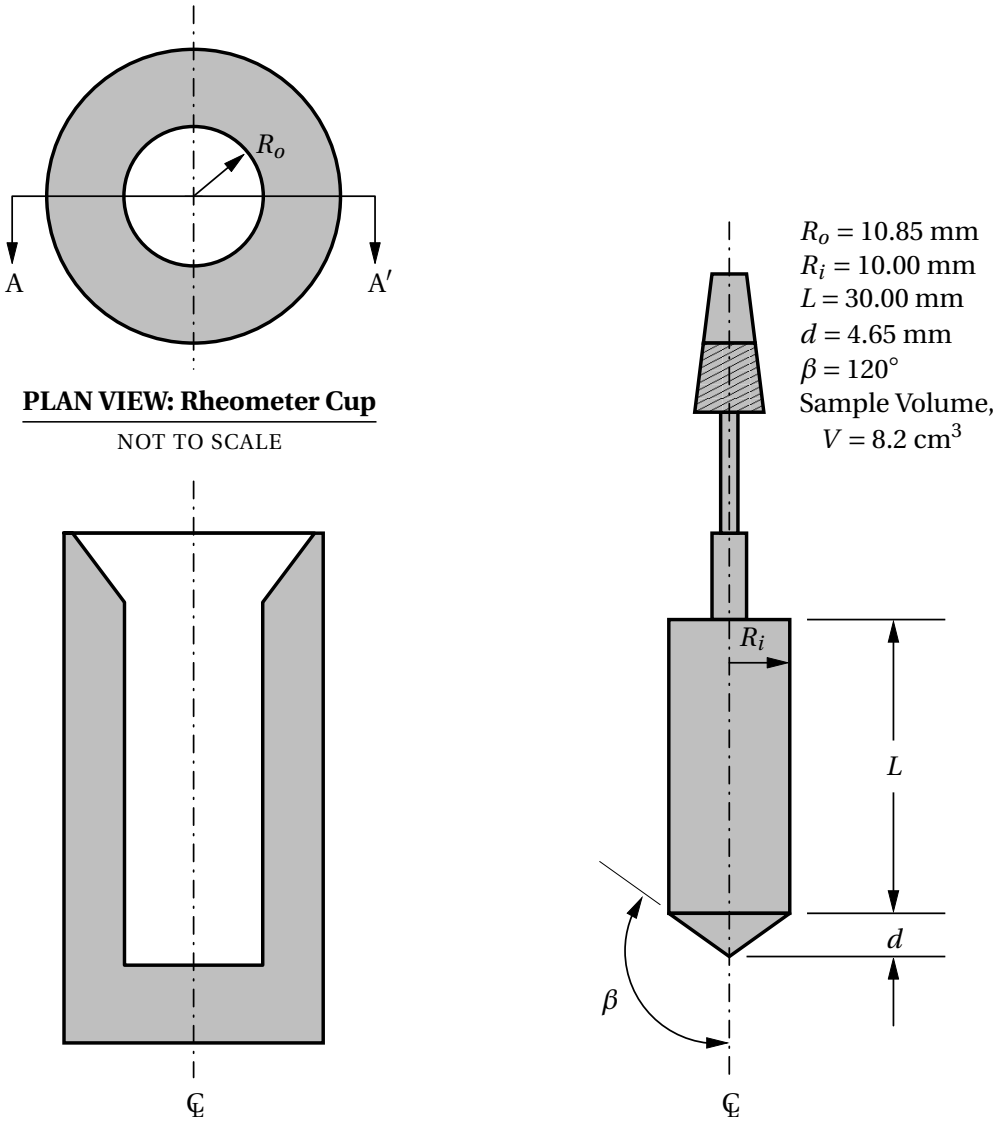

Figure 3.14: Detail of rheometer cup and cone

water and again stored in sealed containers. Vacuum was applied to the samples to remove any air bubbles from the slurry. The samples were then poured into the rheometer cup 24 hours before the test. The settling period of 24 hours was chosen because it has been shown that the yield stress of remolded samples as measured with a rheometer is basically constant between 24 hours and 48 hours after sample preparation (Hoepner, 2000). This also provided an opportunity to observe the qualitative settling characteristics of the slurry. Based on the clarity of the sediment-water interface, the slurry could be classified as flocculated or dispersed as shown in Figure 3.15, following Ravisangar et al. (2005). The rheometer apparatus directly measures the yield stress of the samples.

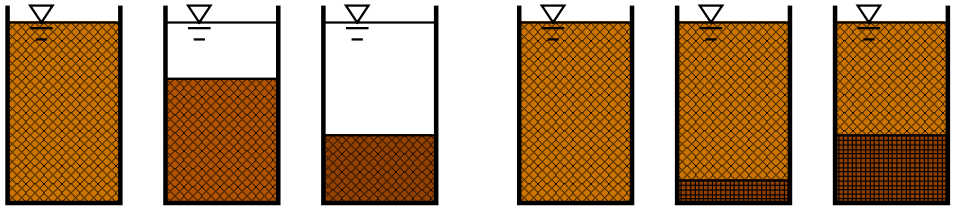

(a) Flocculated, clear interface (b) Dispersed, muddy interface

Figure 3.15: Progression of sediment-water interfaces during settlement

Hoepner (2000) programmed the apparatus to logarithmically increase the shear stress from 0.04 Pa to 12 Pa over a period of 300 seconds. From this procedure, a logarithmic rate factor, Δ, was defined.

$$\Delta = \frac{\log\left(\frac{\tau_{max}}{\tau_{min}}\right)}{t} \tag{3.23}$$

Since some of the current samples to be tested were considerably more resistant to shear than those of the past study, the Δ-factor was kept constant as tests were carried out to higher maximum shear stresses. This resulted in either an increase to 24 Pa over 336 seconds, to 36 Pa over 358 seconds or 48 Pa over 373 seconds. The flow curve is recorded at 20 °C (68 °F) and the apparatus is driven by a pressure of 250 kPa (36.2 psi) provided by compressed air. The lower yield stress (τ_{y1}) is determined from the stress-strain flow

curve by fitting power curves to the inital, low-strain section and also to the brief transition to the high strain portion of the flow curve. The intersection of these two curves is defined as the lower yield stress, as show in Figure 3.16. The upper yield stress (τ_{y2}), as

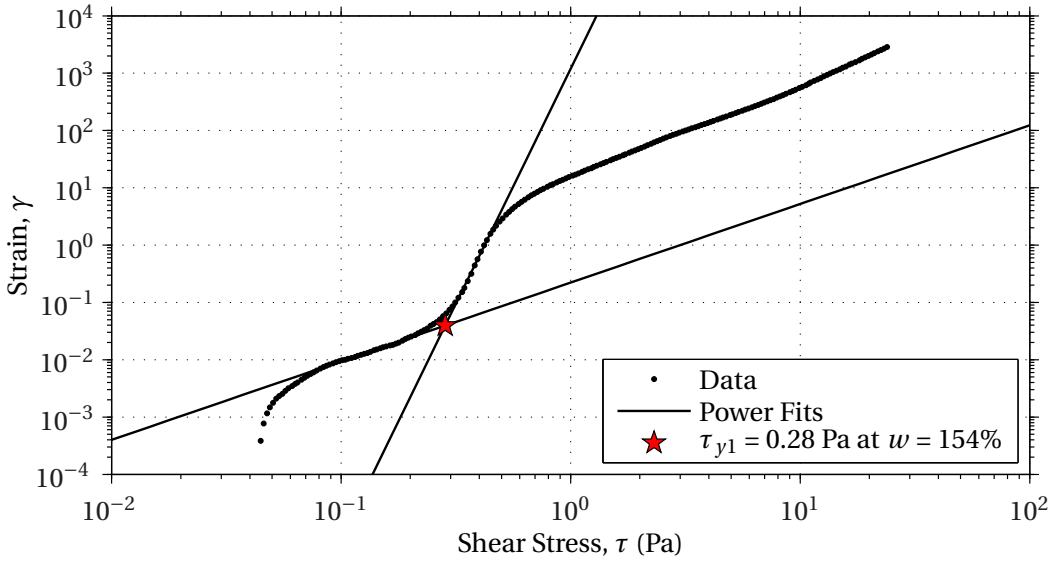

Figure 3.16: Determining the lower yield stress from a stress-strain flow curve

defined by Otsubo and Muraoka (1988) is similarly determined by fitting straight lines to the initial steep and final flatter parts of the strain rate-stress flow curves. This procedure is illustrated in Figure 3.17.

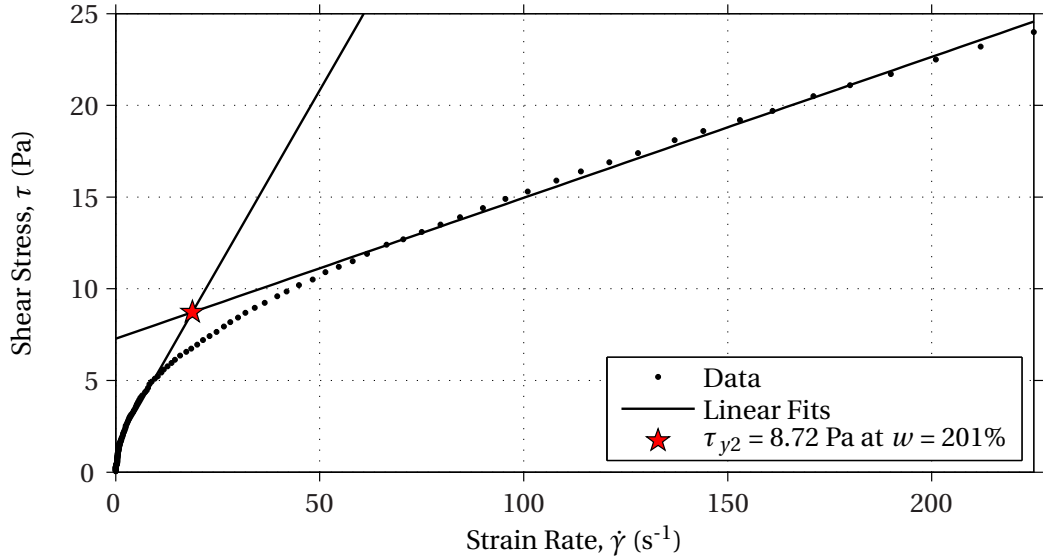

Figure 3.17: Determining the upper yield stress from a strain rate-stress flow curve

CHAPTER IV

RESULTS AND ANALYSIS

4.1 Sediment Properties and Geographic Origin

This section summarizes the results obtained from each sample received from GDOT. The geotechnical characteristics, critical shear stress, and yield stresses of each sample are presented in Table 4.1 through Table 4.5. A brief description of the physical appearance, condition, and behavior of the sample accompanies each table. All of the samples exhibiting plastic behavior are plotted on a standard plasticity chart in Figure 3.11 on page 42. Plots summarizing the results of the erosion and rheological tests will appear in Section 4.2 and Section 4.3, respectively. With few exceptions, the rheometer slurries settled in a flocculated manner as shown in Figure 3.15(a) and flowed in the yield pseudo-plastic manner illustrated in Figure 2.2. These findings are consistent with those of Hoepner (2000). Most often the yield stress decreased with increasing water content (decreasing sediment concentration).

4.1.1 Red Oak Creek in Meriwether County

The first sample analyzed in the laboratory originated from Red Oak Creek at GA 362 in Meriwether County in the Southern Piedmont physiographic region of Georgia. Three Shelby tube samples were collected at 7 ft, 10 ft, and 15 ft below ground surface (BGS). The 7 ft to 9 ft BGS and 10 ft to 12 ft BGS tubes arrived still moist, but only approximately 50% of their length contained soil. Both of these tubes contained gray to brown inorganic sandy silty clays that behaved similarly, although the 10 ft to 12 ft sample was

composed of a slightly finer material. Both materials are low plasticity clays as seen on the plasticity chart in Figure 3.11. Neither sample eroded after several hours at 21 Pa, the maximum bed shear stress obtainable in the flume. As a result, no critical shear stress could be found for either the 7 ft to 9 ft or the 10 ft to 12 ft samples. Three lower and upper yield stress values at different water contents were determined for both of these samples. Meriwether 7 ft to 9 ft behaved unusually by exhibiting slightly increasing lower yield stree with increasing water content. It was also one of the two samples that strongly showed Bingham plastic behavior in its flow curves. The activity and Atterberg limits of these samples fell within the range characteristic of kaolinite, a common mineral in Georgia.

The 15 ft to 17 ft BGS sample was about 80% full, but the bottom of the tube was severely damaged as a result from attempts to push the tube through rock. The damaged section of the tube containing rock was removed and discarded prior to testing. The remaining portion contained two sandy materials that were still moist, though it is entirely plausible that moisture was lost in the few days between collection and testing since the damage tube prevented effective sealing of the tube. The top layer from 15.25 ft to 15.75 ft BGS is classified as a gray, poorly graded sand. The critical shear stress for this material is 1.59 Pa. The final material from this site (16 ft to 16.75 ft BGS), is an orange poorly graded sand. A significant fraction of the material composition was mica, thus its bulk and dry densities are quite low, much like a clay. This soil layer was found to have a critical shear stress of 2.63 Pa. A highly erodible transitional material existed between these two layers, but was completely washed away at the end of the final erosion test of the first layer and could not be characterized further. Neither of the materials found in this Shelby tube contained enough fines to be tested in the rheometer.

Table 4.1 summarizes the results of all three samples from Red Oak Creek in Meriwether County.

Table 4.1: Results from Red Oak Creek in Meriwether County

Depth (BGS)	7 ft to 9 ft	10 ft to 12 ft	15.25 ft to 15.75 ft	16 ft to 16.75 ft
Critical Shear Stress	>21 Pa	>21 Pa	1.59 Pa	2.63 Pa
Lower Yield Stress	0.532 Pa	0.396 Pa	*NP*	*NP*
Upper Yield Stress	12.8 Pa	10.1 Pa	*NP*	*NP*
Sediment	CL	CL	SP-SM	SP
Group Name	Lean clay	Lean clay	Poorly graded sand with silt	Poorly graded sand
Color	Gray with brown	Gray with brown	Gray	Orange
Void Ratio	1.48	0.787	0.926	0.928
Bulk Density	1951 kg/m^3	1910 kg/m^3	2233 kg/m^3	1989 kg/m^3
Dry Density	1435 kg/m^3	1246 kg/m^3	1765 kg/m^3	1478 kg/m^3
Specific Gravity	2.84	2.74	2.68	2.78
Organic Matter	3.15%	4.10%	1.56%	1.77%
Water Content	25.7%	29.1%	26.5%	26.5%
Liquid Limit	31.0	31.7	*NP*	*NP*
Plastic Limit	21.6	20.7	*NP*	*NP*
Plasticity Index	9.4	11.0	*NP*	*NP*
Activity	0.34	0.36	*NP*	*NP*
d_{50}	51 µm	25 µm	0.20 mm	0.90 mm
Sand	45%	36%	93%	95%
Silt	27%	33%	3.5%	2.5%
Clay	28%	31%	3.5%	2.5%

4.1.2 Towaliga River in Monroe County

The next set of samples received from GDOT was collected from the Towaliga River at GA 42 in Monroe County, also located in the Southern Piedmont. Test results are shown in Table 4.2. The first sample from 5 ft to 7 ft BGS is an orange to red with brown clayey sand. The sample occupied roughly 40% of the Shelby tube. Four erosion trials were executed to completion and the critical shear stress of this layer is determined to be 3.77 Pa. Rheometer analysis of the fines of this material resulted in four determinations of upper and lower yield stress that decreased with increasing water content. The slurry settled in a flocculated manner and produced a yield pseudo-plastic flow curve. The activity and Atterberg limits of this sample are consistent with the presence of illite and possibly some kaolinite. Mica was also visually present in the sample. The specific gravity of the soil grains suggests that heavy mineral may have been present.

The second tube from this site was taken from 20 ft to 22 ft BGS. Initially appearing to be very similar to the upper sample, it was in fact comprised of a much finer material. After a couple of erosion trials, the sample began to change materials very quickly. About every 2 cm to 4 cm, the sample would switch from the slowly erodible clay, to a highly erodible sand. Unfortunately, these layers were so thin and erodible, that they would wash out from below the fixed bed whenever the tougher material was either completely removed through surface erosion or experienced a mass failure at high shear stresses. Despite these challenges, erosion data were collected for both materials and the critical shear stresses are found to be 18.38 Pa and 8.76 Pa for the finer and coarser materials, respectively. All attempts to extrude a portion of the sandy material for geotechnical analysis failed, so no geotechnical characterization could be performed on the material. The critical shear stress of the sandy portion of the sample is therefore excluded from the multiple linear regression analyses discussed in Section 4.5. Four lower and three upper yield stress values were determined for this material. The upper yield stress generally

remained constant with water content. The slurry settled in a flocculated manner and produced a yield pseudo-plastic flow curve. The activity and Atterberg limits of this sample are consistent with the presence of kaolinite and possibly illite.

Table 4.2: Results from Towaliga River in Monroe County

Depth (BGS)	5 ft to 7 ft	20 ft to 22 ft (fine/coarse)
Critical Shear Stress	3.77 Pa	18.38 Pa/8.76 Pa
Lower Yield Stress	1.71 Pa	1.08 Pa
Upper Yield Stress	18.1 Pa	13.2 Pa
Sediment	SM	ML
Group Name	Silty sand	Inorganic silt
Color	Orange with brown	Orange with brown
Void Ratio	0.681	1.89
Bulk Density	2050 kg/m^3	2081 kg/m^3
Dry Density	1717 kg/m^3	1345 kg/m^3
Specific Gravity	2.96	2.79
Organic Matter	1.77%	4.80%
Water Content	16.3%	36.0%
Liquid Limit	28.5	45.8
Plastic Limit	22.8	34.3
Plasticity Index	5.7	11.5
Activity	0.57	0.44
d_{50}	0.11 mm	27 µm
Sand	62%	25%
Silt	17%	49%
Clay	20%	26%

4.1.3 Bay Creek in Houston County

After several hours in the flume, no erosion could be achieved in either of the samples from Bay Creek at W. Perry Parkway in Houston County, located in the Sea Island and

East Gulf Coastal Plain. The sample collected at 10 ft to 12 ft BGS was a red to dark red low plasticity clayey sand with very little silt content that is typically associated with the Piedmont region. In the rheometer, Houston 10 ft to 12 ft showed flocculated settling behavior and mostly yield pseudo-plastic flow characteristics, though the slurry with the lowest sediment concentration resembles a Bingham plastic fluid. The activity and Atterberg limits of the sample suggest the possibility of the presence of illite and kaolinite minerals.

The deeper sample from 25 ft to 27 ft BGS was a light gray silty clay with low plasticity. The shallow sample provided four lower yield stresses and three upper yield stresses, all of which decrease with increasing water content. The sediment flocculated in the slurry and flowed as a Bingham plastic fluid. The activity, Atterberg limits, and pale gray color of the sample suggest that the clay minerals may be kaolinite.

Table 4.3 summarizes the results of these samples.

4.1.4 Hodchodkee Creek in Stewart County

Further problems were encountered while testing samples from Hodchodkee Creek at CR 99 in Stewart County, also found in the Sea Island and East Gulf Coastal Plain. The tube taken at 10 ft to 12 ft BGS was heavily corroded, reducing the inner diameter of the tube enough to prohibitively restrict extrusion for erosion testing. Only small portions were extruded with some difficulty for geotechnical analysis. From 10 ft to 11 ft BGS, the sample is a dark brown clayey sand. Below that, there is dark brown poorly graded sand. The fine portion of the sample was tested in the rheometer, but failed to produced reliable flow curves. The clay particles of this sample are mostly inactive. Mica was visually identified and the texture was consistent with other samples containing kaolinite.

Table 4.3: Results from Bay Creek in Houston County

Depth (BGS)	10 ft to 12 ft	25 ft to 27 ft
Critical Shear Stress	>21 Pa	>21 Pa
Lower Yield Stress	2.67 Pa	0.309 Pa
Upper Yield Stress	15.9 Pa	17.7 Pa
Sediment	SC	CL
Group Name	Clayey sand	Silty Clay
Color	Red to dark Red	Light gray with dark streaks
Void Ratio	0.640	0.416
Bulk Density	2363 kg/m^3	1995 kg/m^3
Dry Density	2025 kg/m^3	1428 kg/m^3
Specific Gravity	2.76	2.79
Organic Matter	4.75%	5.30%
Water Content	18.6%	24.7%
Liquid Limit	33.4	35.4
Plastic Limit	14.8	22.1
Plasticity Index	18.6	13.2
Actvity	0.50	0.33
d_{50}	89 µm	7 µm
Sand	53%	27%
Silt	10%	33%
Clay	37%	40%

The second sample tube from 15 ft to 17 ft BGS was similarly corroded, but erosion testing could take place after the tube was cut in half to reduce the friction force needed to be overcome by the piston. Both halves of the remaining sample were composed of similar materials. The lower half (16 ft to 17 ft BGS) contained a large piece of wood that capped the entire cross section of the tube. After this was removed, the erosion rates increased slightly, but the critical shear stress remained essentially the same. An insufficient amount of material remained for a second soil characterization, though initial inspection indicates that the two materials were similar. Neither material contained enough fines for rheologic characterization. A summary of the results for the sample from Stewart County at Hodchodkee Creek are presented in Table 4.4.

4.1.5 Canoochee River in Candler County

Both Shelby tubes from Candler County in the Sea Island region of Georgia contained about 1.5 ft of hard, stiff marine clays that could not be eroded and consisted nearly entirely of clay-sized particles. The soils were so brittle that a level surface could not be cut with a wire saw despite very high *in situ* water contents. Instead, the entire section erratically fractured, leaving an irregular surface with sharp ridges up to 2 cm above the valleys. Much care was taken to create the smoothest surface possible before extruding a portion of the sample to measure the bulk density. Both of these unusual materials were overlain by approximately 0.5 ft of a softer, but equally unerodible material. The more prevalent, harder soils showed a highly expansive nature during the hydrometer analysis when they both formed a semi-solid paste that expanded to fill the entire volume of 250-mL beakers after mixing with the dispersing agent. Strong expansive characteristics were also observed as these samples were rewetted in preparation for the rheometer tests.

As shown in Table 4.5, all four materials had critical shear stresses higher than 21 Pa.

Table 4.4: Results from Hodchodkee Creek in Stewart County

Depth (BGS)	10 ft to 11 ft	11 ft to 12 ft	15 ft to 17 ft
Critical Shear Stress	–	–	1.60 Pa
Lower Yield Stress	*NP*	–	*NP*
Upper Yield Stress	*NP*	–	*NP*
Sediment	SP	SC	SC
Group Name	Poorly graded sand	Clayey sand	Clayey sand
Color	Dark brown	Dark brown	Light brown to white
Void Ratio	0.924	0.963	0.943
Bulk Density	2125 kg/m^3	1927 kg/m^3	2436 kg/m^3
Dry Density	1580 kg/m^3	1258 kg/m^3	2080 kg/m^3
Specific Gravity	2.68	2.68	2.75
Organic Matter	0.97%	9.81%	1.22%
Water Content	28.8%	34.7%	14.6%
Liquid Limit	*NP*	26.6	*NP*
Plastic Limit	*NP*	21.4	*NP*
Plasticity Index	*NP*	5.2	*NP*
Activity	*NP*	0.15	*NP*
d_{50}	0.35 mm	0.10 mm	0.22 mm
Sand	92%	55%	85%
Silt	2%	10%	3%
Clay	6%	35%	12%

Three and five lower and upper yield stresses were measured from the 10 ft to 10.5 ft BGS and 10.5 ft to 12 ft BGS samples, respectively. The upper yield stresses show little downward trend with increasing water content while the lower yield stresses affirmatively decrease with increasing moisture. Only one coherent flow curve could be measured for the 17 ft to 17.5 ft BGS sample. Three lower and upper yield stress values were determined for the sample from 17.5 ft to 19 ft BGS. Both sets sharply decrease with increasing moisture. The dilatancy, or the expansion of clays with moisture, exhibited by these samples is often associated with montmorillonite. The Atterberg limits of the sample from 10.5 ft to 12 ft suggest that montmorillonite dominates the mineralogy of this sample. The Atterberg limits and activities of the other samples indicate that other minerals such as illite and kaolinite were present. Additionally, all four materials were the only samples to settle in a dispersed manner in the rheometer cup. Typical yield-pseudo plastic behavior was found in all four materials.

Table 4.5: Results from Canoochee River in Candler County

Depth (BGS)	10 ft to 10.5 ft	10.5 ft to 12 ft	17 ft to 17.5	17.5 ft to 19 ft
Critical Shear Stress	>21 Pa	>21 Pa	>21 Pa	>21 Pa
Lower Yield Stress	6.02 Pa	2.68 Pa	–	0.494 Pa
Upper Yield Stress	15.9 Pa	17.7 Pa	–	4.83 Pa
Sediment	MH	OH	OH	MH
Group Name	Inorganic silt	Organic clay	Organic clay	Inorganic silt
Color	Bluish gray	Blue to greenish gray	Bluish gray	White to yellowish gray
Void Ratio	1.07	1.85	1.32	1.23
Bulk Density	1794 kg/m^3	1410 kg/m^3	1848 kg/m^3	2030 kg/m^3
Dry Density	805 kg/m^3	635 kg/m^3	729 kg/m^3	1144 kg/m^3
Specific Gravity	2.54	2.45	2.67	2.60
Organic Matter	4.09%	5.44%	3.31%	3.45%
Water Content	71.5%	122.0 %	60.5 %	53.2%
Liquid Limit	71.7	131.5	57.8	55.9
Plastic Limit	61.6	94.6	37.1	43.3
Plasticity Index	10.1	36.9	20.8	12.6
Activity	0.20	0.38	0.49	0.18
d_{50}	2 µm	0.2 µm	4 µm	0.5 µm
Sand	25%	1%	27%	7%
Silt	25%	1%	31%	21%
Clay	50%	98%	42%	72%

4.2 Erosion Relationships

As discussed previously in Chapter 2, several investigators have sought to characterize the eroded material and the eroding flow. These two entities are completely independent and must be treated separately. As is evident upon inspection of Table 2.2, most models of erosion use the difference between the applied bed shear stress (τ) and the critical shear stress of the eroded material (τ_c), known as the excess shear stress. This technique achieves the goal of using independent characteristics of the eroding flow and eroded sediment. After a relationship is established, parameters describing the erosion can then be correlated with other properties of the sediments to investigate any possible dependencies useful to scour prediction.

Navarro (2004) used three models to relate the measured erosion rate, E, to the applied bed shear stress, τ. These models were linear, piece-wise linear, and exponential. Only the linear and exponential models were used in this study as none of the provided samples resulted in a sufficient amount of data to reliably fit a piece-wise linear model. The two applicable models were explored on all seven of the 15 samples that produced suitable erosion test data. Additionally, the suitability of each model was assessed using statistics such as the coefficient of determination (R^2), and the standard errors (SE) of both the models predictions and its parameters.

The linear model (Equation 3.12) is considered to be suitable ($R^2 > 0.50$) in describing all 7 eroded samples. However, the first sample eroded, Meriwether 15 ft to 16 ft BGS, only consists of two data points and is therefore a trivial case. The remaining six samples have coefficients of determination ranging from 0.57 to 0.84. The critical shear stress is determined by extrapolating the best-fit line down to zero erosion. The standard error of this value was calculated. The erosion rate constant, M, was also determined in fitting a linear model to the data. The standard error of M normalized by itself (SE_M/M)

was also calculated ans used as a means of evaluating the goodness-of-fit. The erosion rate data are plotted below in Figure 4.1 and Figure 4.2. The former contains data where the erosion rate (E) was less than 9.0 kg/m^2/s, while the latter contains data with $E < 1.0$ kg/m^2/s. Table 4.6 and Table 4.7 summarize the values of the critical shear stress (τ_c and erosion rate constant for the linear model and the exponential model discussed further below. Due to its asymptotic nature, the exponential erosion model in Equation 3.13

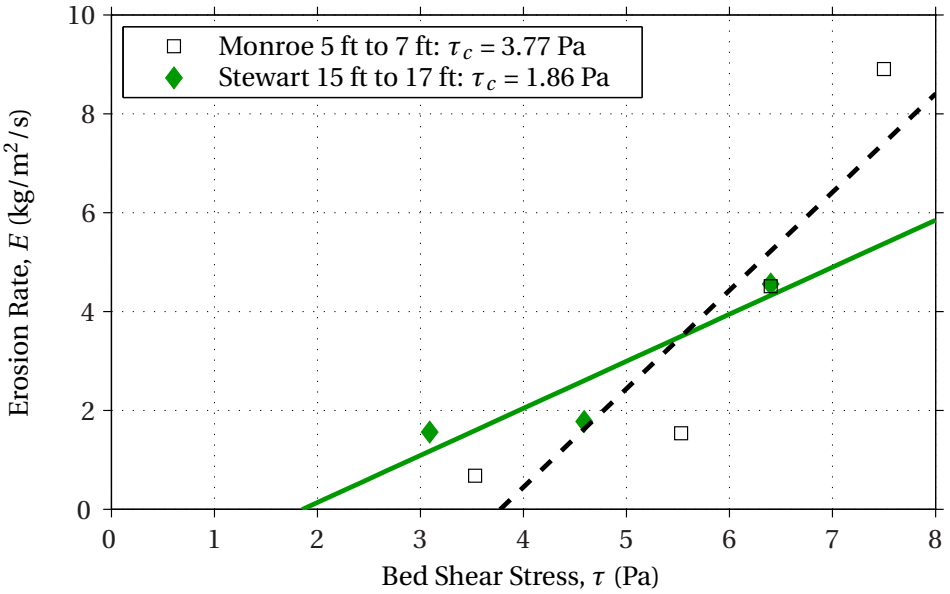

Figure 4.1: Erosion rate vs. bed shear stress with linear fits for $E < 9.0$ kg/m^2/s

requires an additional step before it can be fit to data. Since the model can never predict

Table 4.6: Critical shear stress values and statistics

Sample	Linear			Exponential		
	τ_c (Pa)	SE_{τ_c} (Pa)	R^2	τ_c (Pa)	SE_{τ_c} (Pa)	R^2
Meriwether 15 ft to 16 ft	1.59	0.00	1.00	–	–	–
Meriwether 16 ft to 17 ft	2.63	0.46	0.63	–	–	–
Monroe 5 ft to 7 ft	3.77	1.30	0.81	–	–	–
Monroe 20 ft to 22 ft (1)	18.8	0.34	0.76	18.4	0.25	0.46
Monroe 20 ft to 22 ft (2)	7.33	0.46	0.57	8.76	0.23	0.51
Stewart 15 ft to 17 ft (1)	1.37	0.35	0.84	–	–	–
Stewart 15 ft to 17 ft (2)	1.85	0.89	0.84	–	–	–

Table 4.7: Erosion constants and statistics

Sample	Linear			Exponential		
	M (kg/m^2/s)	SE_M (kg/m^2/s)	$\frac{SE_M}{M}$	a (kg/m^2/s)	SE_a (kg/m^2/s)	$\frac{SE_a}{a}$
Meriwether 15 ft to 16 ft	0.156	0	–	–	–	–
Meriwether 16 ft to 17 ft	0.154	0.175	113%	–	–	–
Monroe 5 ft to 7 ft	7.51	1.28	17.0%	–	–	–
Monroe 20 ft to 22 ft (1)	2.21	0.058	2.62%	34.5	0.25	0.73%
Monroe 20 ft to 22 ft (2)	0.122	0.045	36.8%	6.40	0.23	3.58%
Stewart 15 ft to 17 ft (1)	0.222	0.18	80.6%	–	–	–
Stewart 15 ft to 17 ft (2)	1.77	0.88	48.0%	–	–	–

a shear stress at which zero erosion occurs, a sufficiently small rate of erosion known as the critical erosion rate, E_c, must be chosen. The bed shear stress at which the value occurs is then defined as the critical shear stress. Navarro (2004), using the same procedure and recirculating flume shown in Figure 3.4, selected a value of $E_c = 0.0190$ kg/m^2/s. The reason this value was chosen is twofold: 1) it is of the same order as the minimum erosion rate measurable in the flume; and 2) it produces critical shear stress values comparable to those of the linear model for the samples available. However, when fitting the model to the data, only the samples from Monroe County 20 ft to 22 ft fit in a manner that provided non-negative critical shear stress values. Furthermore, only the coarser fraction of the sample resulted in a suitable fit for the exponential model. As described in Section 4.1, this highly erodible portion of the sample occurred in several very thin layers between thicker layers of a much tougher, finer material. No portion of the material was recovered for a geotechnical characterization. As a result, only the linear model and its resulting parameters are discussed in the remainder of this document. Nonetheless, these data and the exponential fits are presented in Figure 4.3.

Lastly, the critical shear stress values obtained for the best straight line fits were used to determine the Shields parameter using Equation 2.8. These values were then plotted on the Shields diagram in Figure 4.4 with the data of Navarro (2004) and contours of the fines contents of the sediments. The new data points agree fairly well with the previous work. Unfortunately, many of the current data are censored. This means that several critical shear stress values are known only to be *greater than* 21 Pa. Section 5.3 describes the possibility of using highly specialized statistical techniques to handle censored data. However, for the purposes of this report, only the uncensored values will be analyzed in detail.

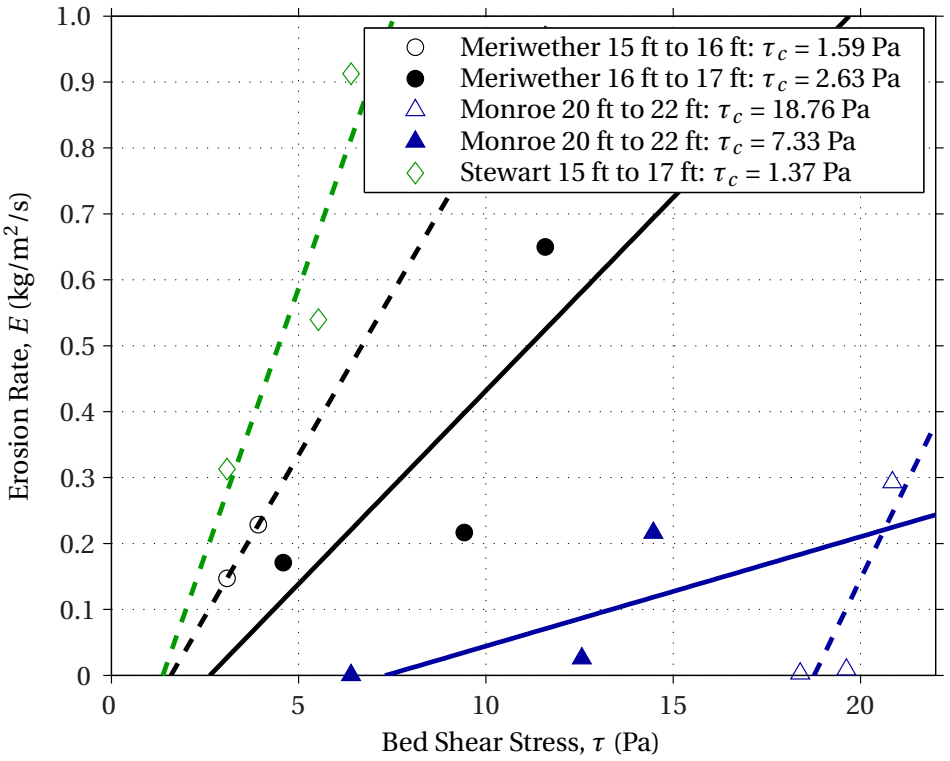

Figure 4.2: Erosion rate vs. bed shear stress with linear fits for $E < 1.0$ kg/m^2/s

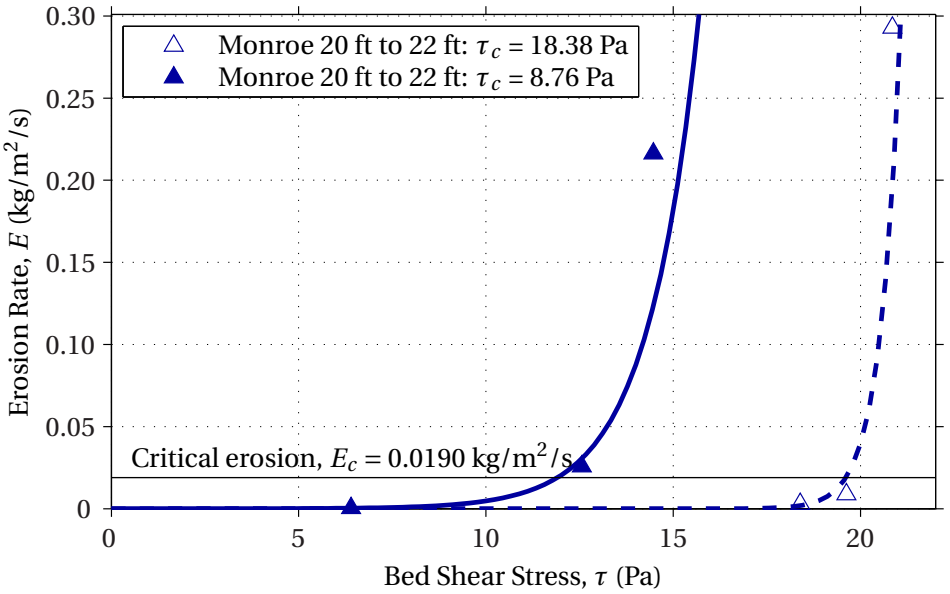

Figure 4.3: Erosion rate vs. bed shear stress with exponential fits

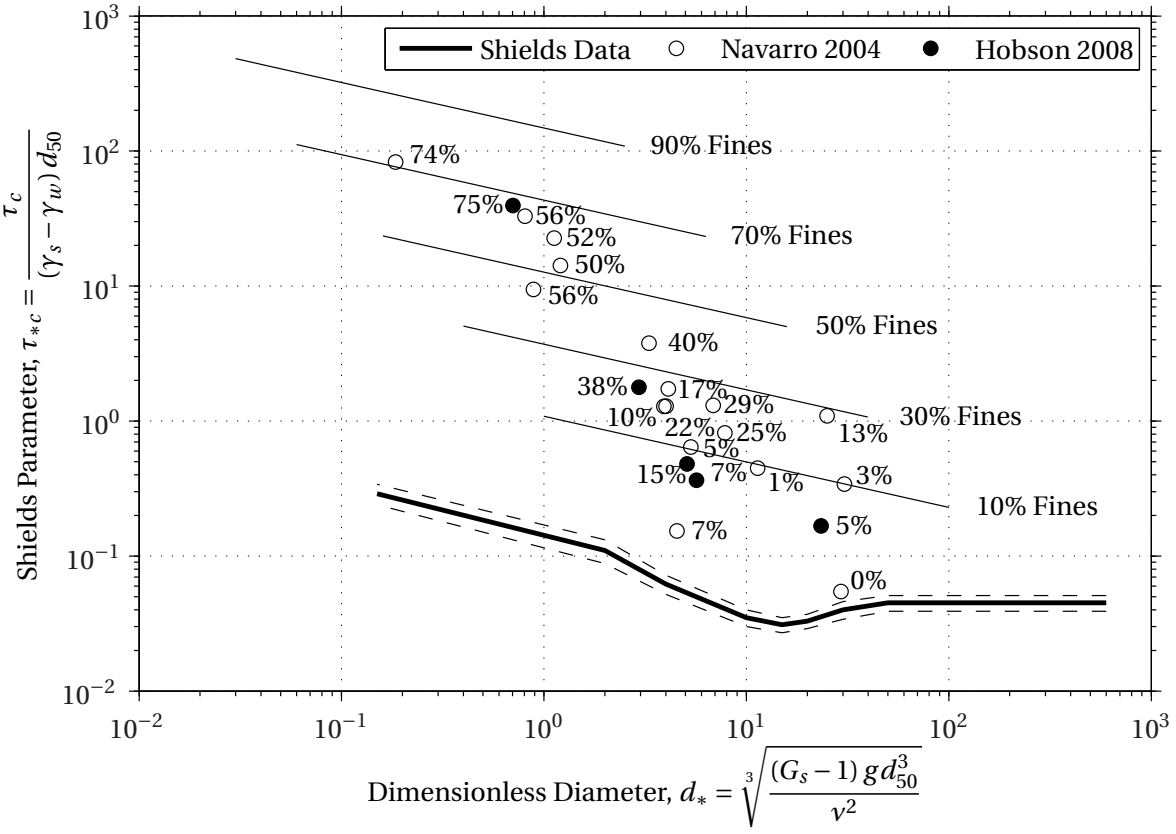

Figure 4.4: Shields diagram with natural sediments

4.3 Yield Stress Relationships

As outlined in Section 3.4.5, the lower and upper yield stresses (τ_{y1} and τ_{y2} of samples that exhibited plastic behavior were determined at varying water contents. In addition, the settling behavior of the suspension was also observed by characterizing the sediment-water interface as sharp (flocculated) or muddy (dispersed). Figure 4.5(a) and Figure 4.5(b) separate and summarize the lower yield stress values for all of the flocculated and dispersed suspensions, respectively. These figures clearly show the differing natures of the types of suspension. In Figure 4.5(a), over a range of water contents from

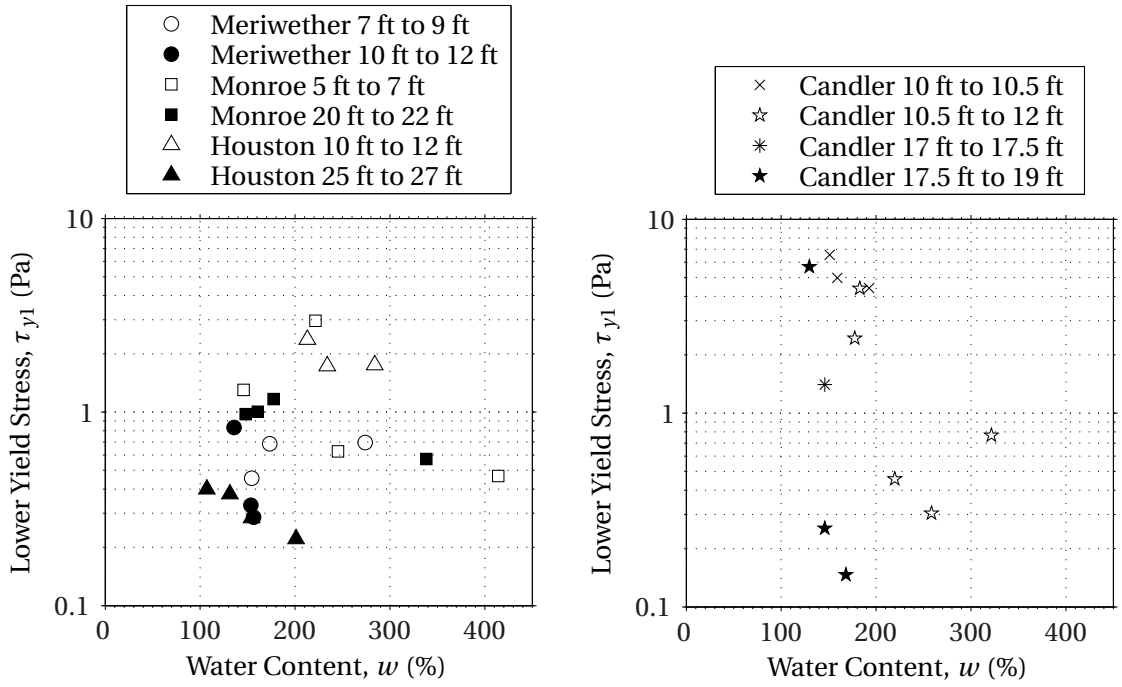

(a) Lower yield stress, flocculated

(b) Lower yield stress, dispersed

Figure 4.5: Measured lower yield stress results of (a) flocculated and (b) dispersed sediment slurries as functions of water content

100% to 425%, all samples yield within 0.2 Pa and 1.3 Pa, or a range of roughly one order of magnitude. The dispersed samples yield between 0.12 Pa and 7 Pa over a range of water contents between 100% and 325%. Also notice that the general trend in the flocculated samples exists is flat or slightly decreasing with respect to water content. The

dispersed samples all show very sharp decreasing trends with respect to water content except for Candler 10 ft to 10.5, for which the upper yield stress varies little with water content.

Figure 4.6 presents the upper yield stress results for flocculated and dispersed samples. The same aforementioned trends with respect to water content exist in the upper yield stress data. The flocculated data in Figure 4.6(a) range from 7 Pa to 20 Pa, and the dispersed data in Figure 4.6(b) range from about 1 Pa to 20 Pa.

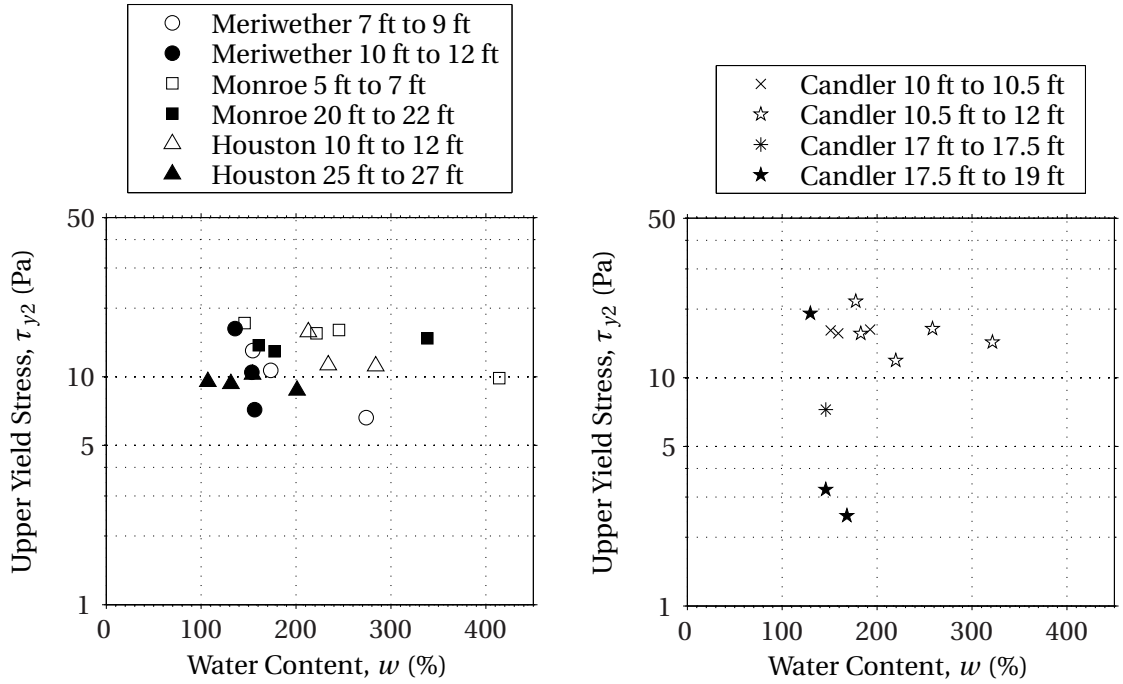

(a) Upper yield stress, flocculated

(b) Upper yield stress, dispersed

Figure 4.6: Measured upper yield stress results of (a) flocculated and (b) dispersed sediment slurries as functions of water content

For each material, the yield stress as a function of water content was plotted with a best-fit straight line. Exponential curves were also fit to the data for statistical examination. Due to the nature of the rheometer test, the yield stress of the sediments could only be measured at water contents significantly higher than those found *in situ*. Thus, the empirical relationships with water content were used to estimate the yield stress at a

standard, yet arbitrary water content of 150% as show in Figure 4.7 for consistent comparisons. This value of water content was selected since it fell into the range of all of

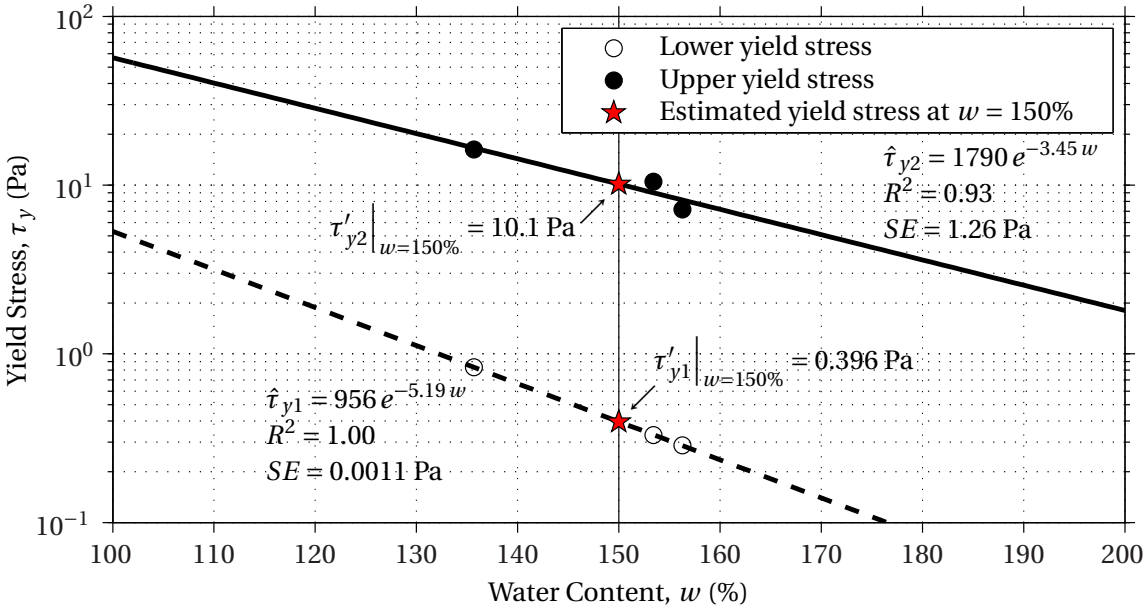

Figure 4.7: Determining the reported yield stresses

the yield stress data. The reported values of lower and upper yield stress, denoted as τ'_{y1} and τ'_{y2}, the coefficients of determination, and the standard errors of the regressions are summarized in Table 4.8 and Table 4.9.

Typically, the measured upper yield stress values were about a factor of two to an order of magnitude greater than the corresponding lower yield stresses. Both sets of yield stress values fit linear and exponential curves reasonably well, though very poor fits in one dataset usual correspond to a good fit in the other. For example, the linear model of Monroe County from 5 ft to 7 ft has an $R^2 = 0.22$ for the lower yield stress, but $R^2 = 0.95$ for the upper. Similarly, the exponential fits of Houston 25 ft to 27 ft have R^2 values of 0.94 and 0.20 for the lower and upper yield stress, respectively. Samples such as Meriwether 10 ft to 12 ft, Monroe 20 ft to 22 ft, and Candler 17.5 ft to 19 ft have similarly good fits. When normalized by the estimated yield stress at $w = 150\%$, the upper yield stress

Table 4.8: Summary of lower yield stress regressions

Sample	Linear Fit				Exponential Fit			
	τ'_{y1} (Pa)	R^2	SE (Pa)	$\frac{SE}{\tau'_{y1}}$	τ'_{y1} (Pa)	R^2	SE (Pa)	$\frac{SE}{\tau'_{y1}}$
Meriwether 7 ft to 9 ft	0.542	0.42	0.10	0.19	0.532	0.41	0.11	0.20
Meriwether 10 ft to 12 ft	0.441	1.00	0.017	0.039	0.396	1.00	0.0011	0.0028
Monroe 5 ft to 7 ft	1.85	0.22	1.01	0.55	1.71	0.16	1.05	0.61
Monroe 20 ft to 22 ft	1.07	0.79	0.12	0.11	1.08	0.76	0.12	0.12
Houston 10 ft to 12 ft	2.61	0.50	0.26	0.097	2.67	0.53	0.25	0.094
Houston 25 ft to 27 ft	0.318	0.94	0.020	0.063	0.309	0.94	0.020	0.064
Candler 10 ft to 10.5 ft	6.05	0.68	0.63	0.10	6.02	0.70	0.61	0.10
Candler 10.5 ft to 12 ft	3.27	0.44	1.30	0.40	2.68	0.60	1.29	0.48
Candler 17.5 ft to 19 ft	1.75	0.68	1.79	1.02	0.494	0.97	1.63	3.29
AVG:	–	0.58	1.65	0.41	–	0.62	1.68	0.91

Table 4.9: Summary of upper yield stress regressions

Sample	Linear Fit				Exponential Fit			
	τ'_{y2} (Pa)	R^2	SE (Pa)	$\frac{SE}{\tau'_{y2}}$	τ'_{y2} (Pa)	R^2	SE (Pa)	$\frac{SE}{\tau'_{y2}}$
Meriwether 7 ft to 9 ft	12.6	0.95	0.73	0.058	12.8	0.97	0.58	0.046
Meriwether 10 ft to 12 ft	10.7	0.94	1.08	0.10	10.1	0.93	1.26	0.12
Monroe 5 ft to 7 ft	17.7	0.95	0.73	0.042	18.1	0.91	1.00	0.055
Monroe 20 ft to 22 ft	13.2	0.73	0.47	0.035	13.2	0.73	0.47	0.036
Houston 10 ft to 12 ft	17.7	0.55	1.75	0.099	18.3	0.59	1.70	0.093
Houston 25 ft to 27 ft	9.44	0.21	0.56	0.059	9.42	0.20	0.56	0.060
Candler 10 ft to 10.5 ft	15.9	0.29	0.27	0.017	15.9	0.30	0.27	0.017
Candler 10.5 ft to 12 ft	18.1	0.19	3.22	0.18	17.7	0.20	3.22	0.18
Candler 17.5 ft to 19 ft	7.45	0.70	5.12	0.69	4.83	0.91	4.24	0.88
AVG:	–	0.55	2.73	0.19	–	0.57	2.68	0.22

values have a lower average standard error, although the average coefficient of determination is higher for the lower yield stresses. The estimated yield stress values at 150% are reported from the exponential regressions. Since the statistics associated with individual fits are so similar, the yield stresses estimated from the expontential curves are selected since they produced more accurate models resulting from the multiple linear regression analyses discussed in Section 4.6.

4.4 Multiple Linear Regression Analysis

Navarro (2004) used the same tilting, recirculating flume to determine the critical shear stress of sediments from other bridge foundations from around Georgia as shown in Figure 3.2. The critical shear stresses of 17 of the 30 materials tested were able to be determined. Using statistical software, Navarro (2004) developed two equations to predict the critical shear stress and one equation for the Shields parameter based on three predicting variables. These equations will be discussed in more detail in Section 4.5.

Many geotechnical properties were tested during the characterization of the soils received from GDOT during this study and the previous one (Navarro, 2004). Chapter 3 details the full extent of the geotechnical characterization. Of the geotechnical values determined, only the following were included as possible predictors in the multiple linear regression analysis:

- bulk density (kg/m^3)
- water content (decimal fraction)
- organic matter content (decimal fraction)
- median particle size (mm)
- clay content (decimal fraction by mass)

- fines content (decimal fraction by mass).

For reasons discussed in Section 4.2, the critical shear stress as determined using the linear regression model was used as the response variable.

The remaining variables were excluded for a variety of reasons. Most notably, specific gravity was excluded since it varies so little (2.4 - 2.8, with the exception of Monroe 5 ft to 7 ft) among soils with drastically different erosion characteristics. Moreover, all the Atterberg limits were excluded since they can only be determined for samples with enough fines to behave in a plastic manner.

The most influential of the above predictors were selected using a best subsets regression. For the best subsets analysis, the statistical software, MATLAB code in this case, starts with a single-variate linear regression and progresses through all possible combinations of predictors input into the program. A stepwise regression adds and removes variables based on their influence relative to other variables (Navarro, 2004). The goodness-of-fit of the resulting models was then assessed using the adjusted coefficient of determination (R^2_{adj}), Mallows' C_p, and the estimated standard error of the models.

The coefficient of determination is a measure of how much variability for which the regression accounts. Following Navarro (2004), R^2 is determined in the manner described below. For the purposes of the discussion in this section, y, $\bar{y}$, and $\hat{y}$ represent a generic dendent variable, its mean, and its predicted values resulting from a regession of y on the indepedent variable x, respectively. The coefficient of determination of this regression is given by:

$$R^2 = \frac{SS_R}{SS_T} = 1 - \frac{SS_E}{SS_T} \tag{4.1}$$

where SS_R is the sum of the squares of the explained deviations of $\hat{y}$ from $\bar{y}$; SS_E is the sum of the squares of the unexplained deviations of y from $\hat{y}$; and SS_T is the total sum of the squares measuring the total variability in y. Mathematically, these values are written

as:

$$SS_T = \sum_{i=1}^{n} \left(y_i - \bar{y}\right)^2 \tag{4.2}$$

$$SS_R = \sum_{i=1}^{n} \left(\hat{y}_i - \bar{y}\right)^2 \tag{4.3}$$

$$SS_E = \sum_{i=1}^{n} \left(y_i - \hat{y}\right)^2 \tag{4.4}$$

where n is the total number of observations and i refers to a particular observation number.

When a linear regression uses multiple predicting variables, R^2 is overestimated using Equation 4.1. R^2 increases because more predictors yield a more accurate model, but decrease the predictability of the response variable. Accounting for the degrees of freedom of the regression provides a more accurate statistic, R^2_{adj}, for assessing the goodness-of-fit of multiple linear regression with k predicting variables.

$$R^2_{adj} = 1 - \left(\frac{SS_E}{SS_T}\right)\left(\frac{n-1}{n-k-1}\right) \tag{4.5}$$

Mallows' C_p also measures the ability of the model's selected independent variables to predict the dependent variable. A good fit is indicated by a C_p value that is small and close to the number of independent variables in the model (k). Mallows' C_p can be calculated as

$$C_p = \frac{SS_{E,k}}{SS_{E,all}/\left(n - k_{all} - 1\right)} - (n - 2k) \tag{4.6}$$

where $SS_{E,k}$ is the sum of the squares of error for the model being evaluated, k is the number of predictors used in the model; $SS_{E,all}$ is the sum of the square of error with all available predictors; and k_{all} is the total number of available predictors. It is clear from Equation 4.6 that values of C_p vary depending on how many predictors are selected as candidates to be included in the model. In other words, omitting any of the predictors listed above would have resulted in different C_p values for the same models. As such,

this statistic and R^2_{adj} were only used to compare different regressions evaluated from the same set of possible predicting variables.

The final statistic used to assess a model's fit was the standard error, SE. This statistics is the average of the errors of the regression model. When used to describe a multiple linear regression, the number of predictors must be accounted for. Equation 4.7 below was used to calculate the standard error of the regressions.

$$SE = \sqrt{\frac{SS_E}{n-k-1}} \tag{4.7}$$

4.5 Predicting Critical Shear Stress from Sediment Properties

The investigation of Navarro (2004) led to the development of two equations that use three soil properties as predictors of the critical shear stress. They both use the fines content and organic matter, then either the median particle size or bulk density as predictors. The first critical shear stress prediction equation was erroneously printed. It appears in corrected form below as Equation 4.8. The other prediction equation appears as originally published.

$$\hat{\tau}_c = 0.744 + 25.9\,\text{Fines} - 62.1\,OM + 2.39\,d_{50} \tag{4.8}$$

$$\hat{\tau}_c = 5.18 + 22.8\,\text{Fines} - 62.8\,OM - 0.00158\,\rho_b \tag{4.9}$$

As show in Table 4.10, the two models provided nearly equally good fits to the data.

Table 4.10: Summary of critical shear stress regression models

Equation	R^2	R^2_{adj}	C_p	SE
4.8	0.72	0.65	1.4	2.64
4.9	0.70	0.63	1.8	3.12

However, examining Equation 4.9 reveals that it negatively relates the critical shear stress to the bulk density, contradicting the past finding of many researchers (Mehta, 1991;

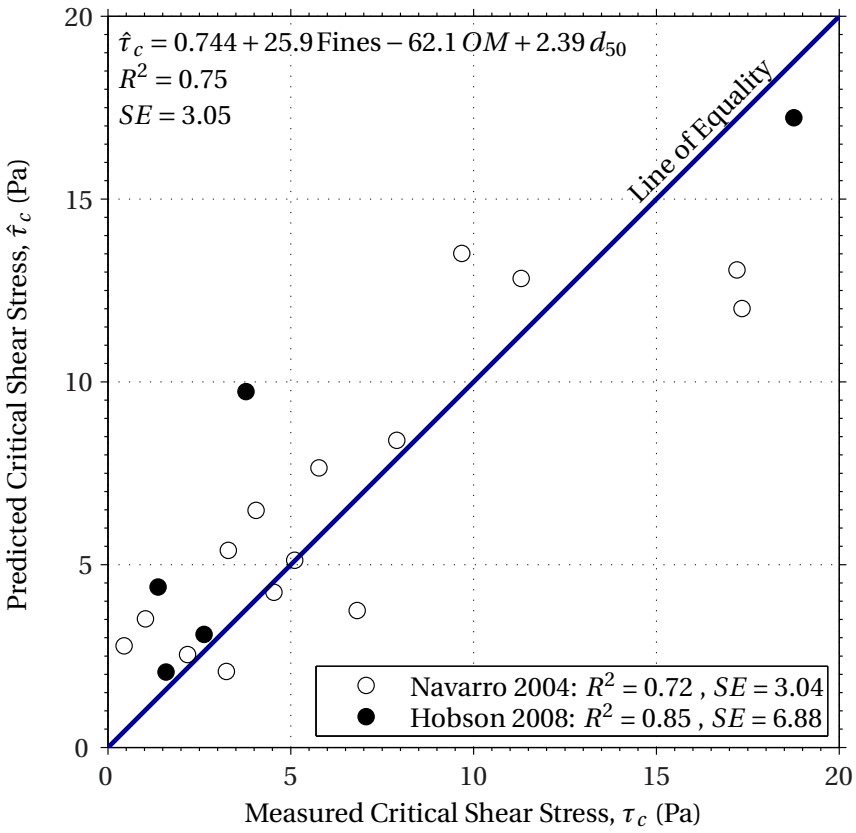

Figure 4.8: Predicting critical shear stress with original model (Equation 4.8)

Krone, 1999; Ravisangar et al., 2001; Briaud et al., 2001). For this reason, Equation 4.8 was selected as the best relationship. The model was then independently applied to the data collected during this study. Figure 4.8 shows a plot of the predicted critical shear stress ($\hat{\tau}_c$) vs. the measured critical shear stress (τ_c). The model does not fit the new data as well as the old data, though the agreement is still adequate. As a general rule, the model over-predicts the critical shear stress of the new data.

A new model was then fit to a combined dataset of values obtained by Navarro (2004) and this study, resulting in Equation 4.10.

$$\hat{\tau}_c = -0.303 + 26.6\,\text{Fines} - 55.7\,OM + 3.23\,d_{50} \tag{4.10}$$

Figure 4.9 shows the new predicted values of critical shear stress plotted against the measured values. Judging from the statistics used to assess the goodness-of-fit, this new

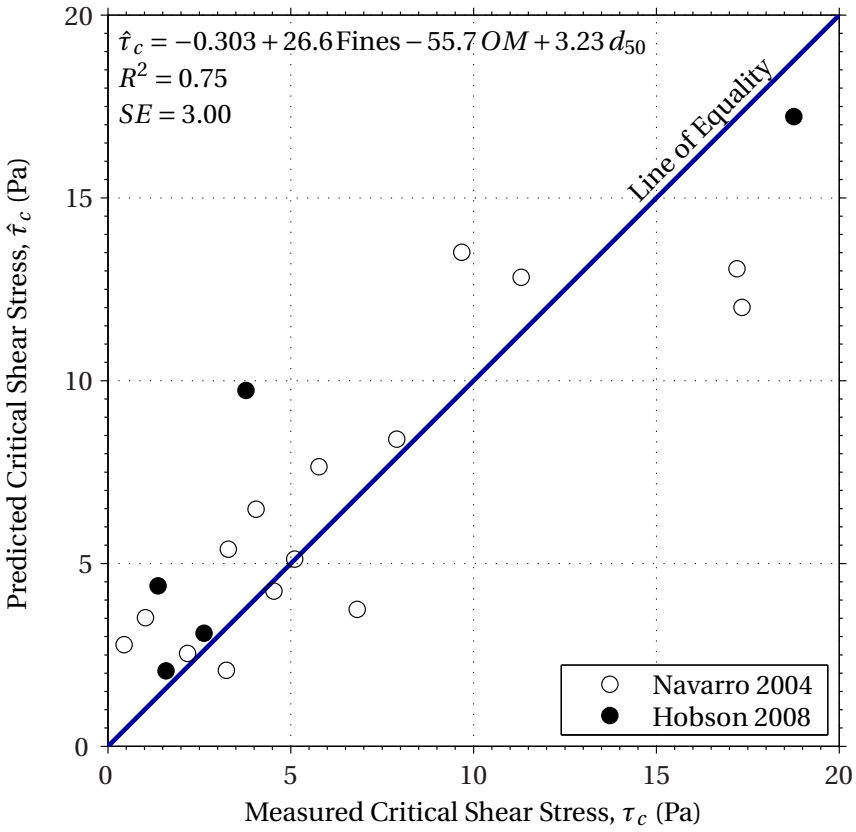

Figure 4.9: Predicting critical shear stress with updated model (Equation 4.10)

model performs better or just as well as Equation 4.8 presented by Navarro (2004).

Also by using a best subsets regression, Navarro (2004) additionally developed an equation to predict the Shields parameter (τ_{*c}) from the fines content and dimensionless particle diameter, d_*.

$$\hat{\tau}_{*c} = 0.584 \times 10^{2.68\,\text{Fines}}\, d_*^{-0.337} \tag{4.11}$$

Figure 4.10 shows the relationship between the predicted and measured Shields parameters of Equation 4.11 applied to both datasets. The model proposed by Navarro (2004) is consistent with the new data as illustrated by the comparable coefficients of determination. After combining both datasets, the regression was performed once again, yielding Equation 4.12 and Figure 4.11 below.

$$\hat{\tau}_{*c} = 0.644 \times 10^{2.68\,\text{Fines}}\, d_*^{-0.409} \tag{4.12}$$

Combining the datasets modifies Equation 4.11 only slightly, and allows for a better fit of both datasets, though the coefficient of determination is highest when the original model is applied to the original data of Navarro (2004) only. The coefficients of the fines content and d_* change very little from Equation 4.11 to Equation 4.12.

Lastly, unique to this study, the median particle size was removed as a predictor of the Shields parameter and a regression was performed using only the fines content of the soil. The rationale behind this decision was that the cohesive nature of the soil is better represented by the fines alone and that d_* might be a redundant predictor. The resulting relationship is shown below as Equation 4.13.

$$\hat{\tau}_{*c} = 0.211 \times 10^{3.35\,\text{Fines}} \tag{4.13}$$

Figure 4.12 shows the predicted Shields parameters plotted against the measured Shields parameters in a manner similar to previous relationships. However, since only one predictor is used, the data can also plotted with the best-fit curve as show in Figure 4.13.

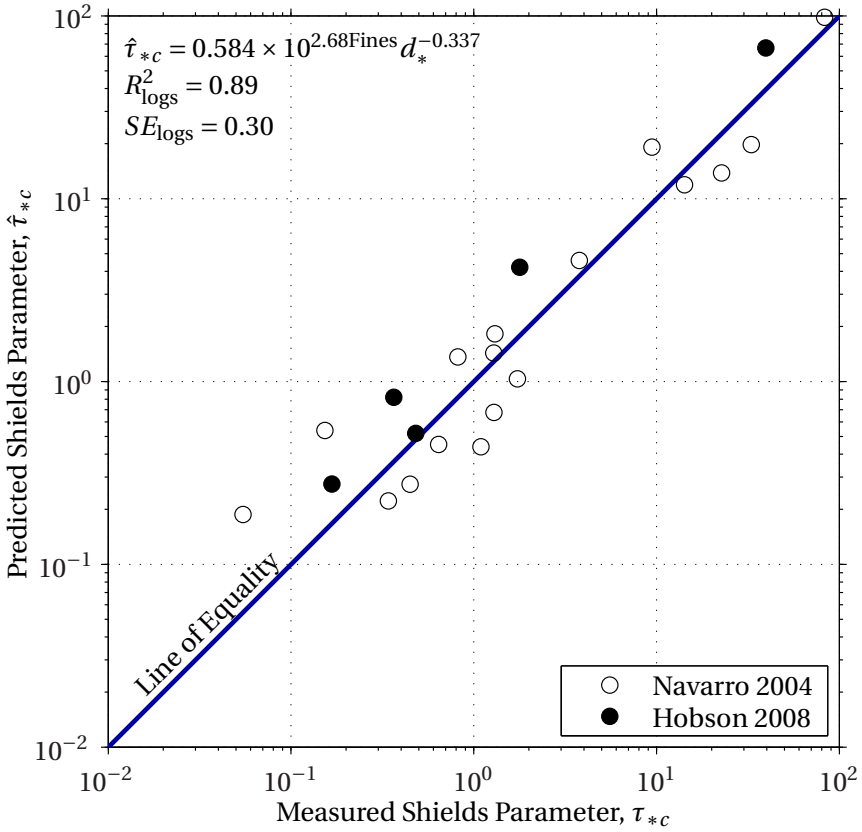

Figure 4.10: Predicting the Shields parameter with original model (Equation 4.11)

Using fines alone gives similar regression statistics, but the viscous influence is lost. Table 4.11 below summarizes the three models developed to predict the Shields parameter of the samples. Despite the ability of Equation 4.13 to predict the Shields parameter us-

Table 4.11: Summary of models predicting the Shields parameter

Equation	Input Data		Parameters Used		Statistics	
	Past	Current	d_{50}	Fines	R^2_{logs}	SE_{logs}
4.11	✓		✓	✓	0.89	0.30
4.12	✓	✓	✓	✓	0.90	0.28
4.13	✓	✓		✓	0.88	0.30

ing only the fines content of the sediment, this neglects the flow's viscous influence on the erosion process provided by d_* in Equations 4.11 and 4.12. This contribution of the prediction of the Shields parameter is valuable and should be maintained. Equation 4.12

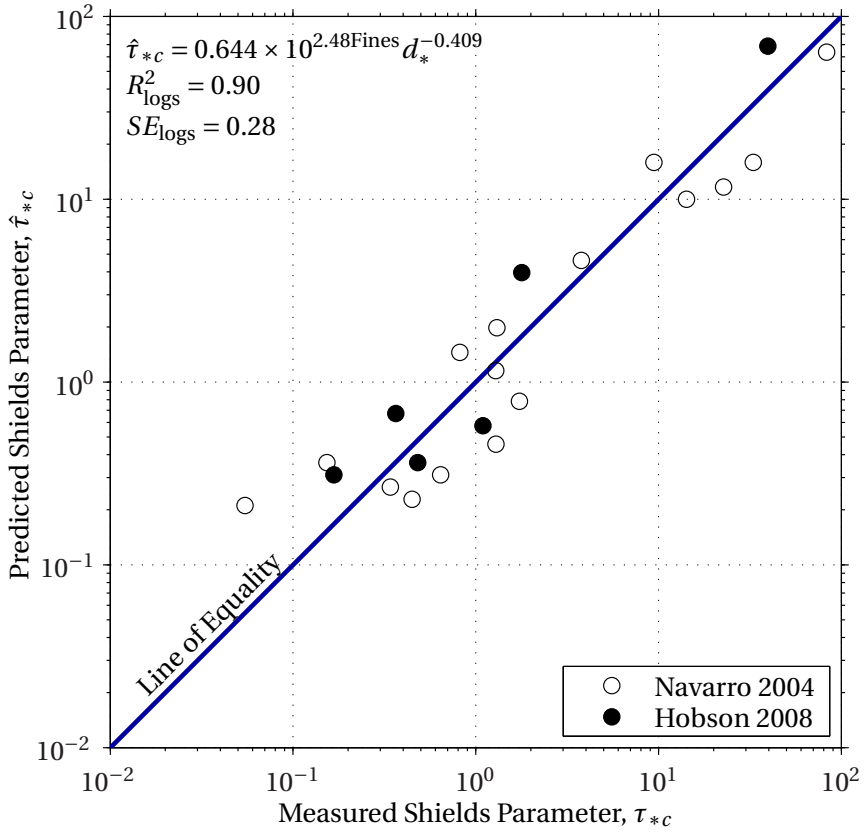

Figure 4.11: Predicting the Shields parameter with updated model (Equation 4.12)

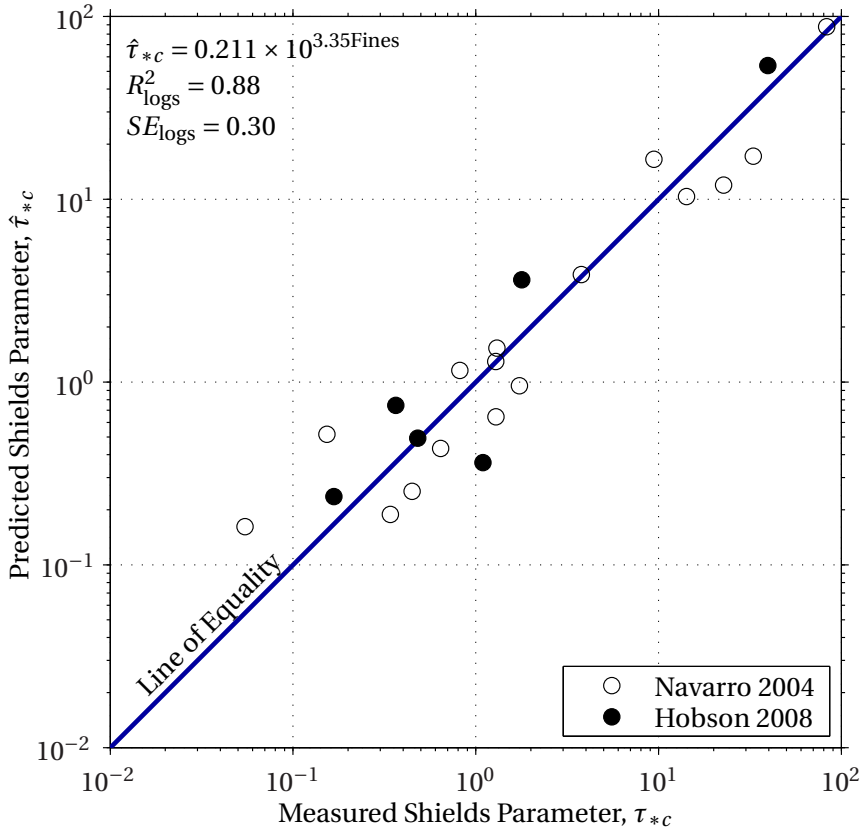

Figure 4.12: Predicting the Shields parameter with fines content (Equation 4.13)

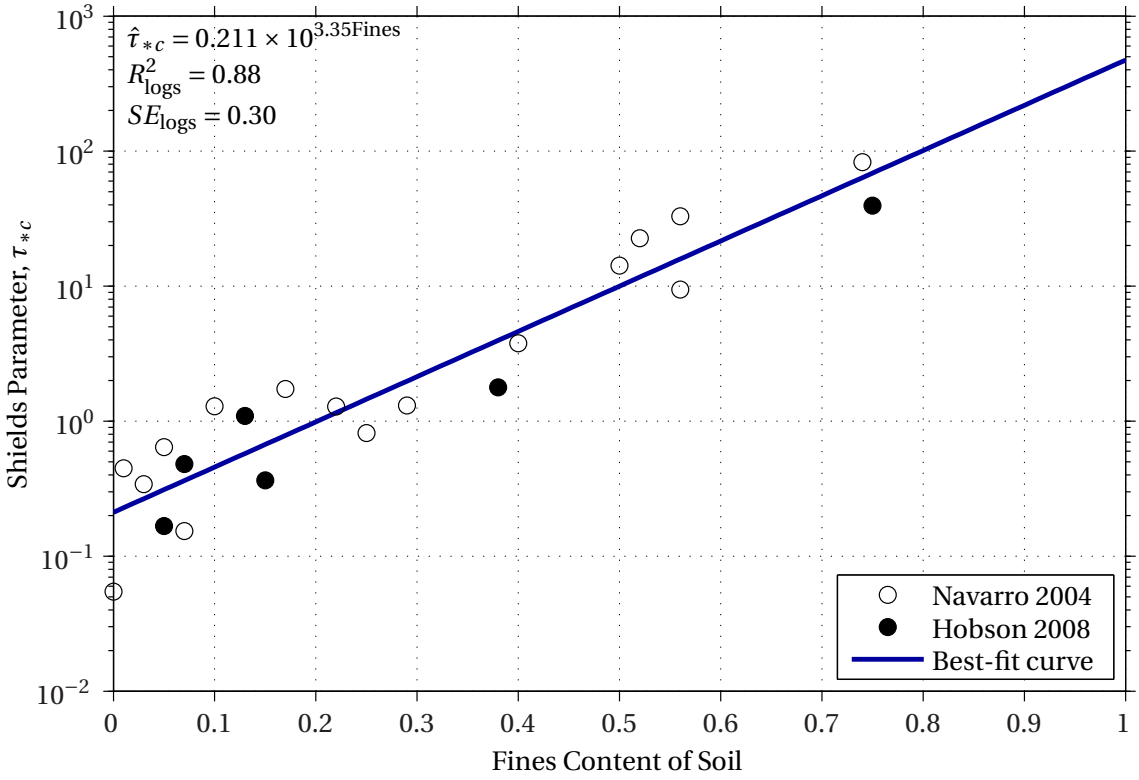

Figure 4.13: Shields parameter plotted as a function solely of fines content (Equation 4.13)

is the best predictor of the Shields parameter of the equations presented here. It should be noted that Equation 4.12 only applies to Georgia sediments with fines contents less than 75% and d_* values ranging from 0.2 to 30.

4.6 Predicting Yield Stress from Sediment Properties

Due to the censored state of the current shear stress data, it is not currently possible to formulate any meaningful direct relationship between the critical shear stress and the yield stresses of the sediments. This problem is exacerbated by the fact that most of the samples that were erodible in the flume were non-plastic and therefore could not be tested in the rheometer. However, the abundant yield stress and geotechnical data for the remaining samples provide for the formulation of models to predict the rheological properties of the fines of the plastic sediments.

Several different regressions were performed to find a sufficiently robust fit. The estimated yield stresses (τ'_y at w = 150% from both linear and exponential curves failed to provide an acceptable fit (R^2 >0.50) for any combination of predictor variables. The values of Mallows' C_p were typically an order of magnitude greater than the number of predictors used in a particular model. In search of a solution, the reported yield stresses were used to compute a modified Shields parameter, or dimensionless yield stress, shown below in Equation 4.14.

$$\tau^*_y = \frac{\tau'_y}{\left(\gamma_s - \gamma_w\right) d_{50}} \tag{4.14}$$

Through a stepwise regression of the following parameters:

- clay content (decimal fraction by mass)
- liquid limit (decimal fraction)
- plastic limit (decimal fraction)
- activity
- dimensionless particle diameter (d_*) and $\log(d_*)$

a single-parameter model based on d_* was selected as the best predictor of both the lower and upper dimensionless yield stresses. Since the sediments tested in the rheometer were completely remolded and had been wet sieved, other geotechnical properties such as water content and bulk or dry density could not be included in the model. In this case, the reported yield stresses estimated from the exponential curves at a water content of 150% produced the best models. This is advantageous for several important reasons. First, the exponential fits provided slightly better statistics than the linear fits. Moreover, as the sediment concentration approaches zero, the yield stress of the suspension should also tend toward zero as the sediment particles lose their influence. The exponential model of yield stress as a function of water content captures this behavior and asymptotically approaches zero. The linear model instead plunges down into physically meaningless negative values at high water contents. For these reasons the yield stress estimated from the exponential curves as shown in Figure 4.7 at a water content of 150% were chosen as the response variable for the model and reported as the yield stress values in Table 4.1 through Table 4.5.

The general form of the model, shown in Equation 4.15, predicts the response variable well with correlation coefficients of 0.85 and 0.97 for the lower and upper dimensionless shear stress, respectively. In the model, A_y and C_y are dimensionless constants.

$$\hat{\tau}_y^* = A_y \, d_*^{C_y} \tag{4.15}$$

The model based on d_* was chosen for the following reasons: 1) it performs satisfactorily for both lower and upper dimensionless yield stresses; 2) using only two predictor variables prevents artificially good fits due to over-parameterization; and 3) it results in the best coefficients and standard errors compared to all other two-parameter models. The resulting equations for the lower and upper dimensionless yield stress appear in Equation 4.16 and Equation 4.17, respectively.

$$\hat{\tau}_{y1}^* = 1.45 \times 10^6 \, d_*^{-3.04} \tag{4.16}$$

$$\hat{\tau}^*_{y2} = 5.30 \times 10^6 \, d_*^{-2.78} \tag{4.17}$$

The models selected to predict the lower and upper dimensionless yield stresses have several attractive characteristics. First and foremost, their high coefficients of determination (0.85 and 0.97) indicate that the models predict the values with little error or bias. The parameters used in the model are also advantageous. The Shields diagram relates the Shields parameter (τ_{*c}) to the dimensionless diameter (d_*). This makes it quite convenient for the dimensionless yield stress, as determined from Equation 4.14, to also relate to d_*. Excluding the fines for the model is also preferential since the samples had been wet sieved, removing any sand. In essence, all of the samples in the rheometer cup were 100% fines. The dimensionless diameter (d_*) is calculated from the median particle size (d_{50}), providing some influence of the grain size distribution of the sediments. Figure 4.14 and Figure 4.15 plots the agreement between the measured dimensionless yield stress and those predicted by Equation 4.16 and Equation 4.17. Note that by using Equations 4.12, 4.16 and 4.17, the Shields parameter and dimensionless yield stresses can be related by the dimensionless particle diameter. The equation for the Shields parameter take the general form shown in Equation 4.18:

$$\hat{\tau}_{*c} = A_c \times 10^{B_c \text{Fines}} d_*^{C_c} \tag{4.18}$$

where A_c, B_c, and C_c are constants. The general form of the equation for the dimensionless yield stress is shown in Equation 4.15 on page 83. By solving both equations for d_* and setting them equal to each other, the Shields parameter can be predicted from the dimensionless yield stress, dimensionless particle diameter and the percect fines by mass of the sediment:

$$\hat{\tau}_{*c} = A_c \times 10^{B_c \text{Fines}} \left(\frac{\hat{\tau}^*_y}{A_y} \right)^{\frac{C_c}{C_y}} \tag{4.19}$$

With the findings from this study, Equations 4.20 and 4.21 predict the Shields parameter

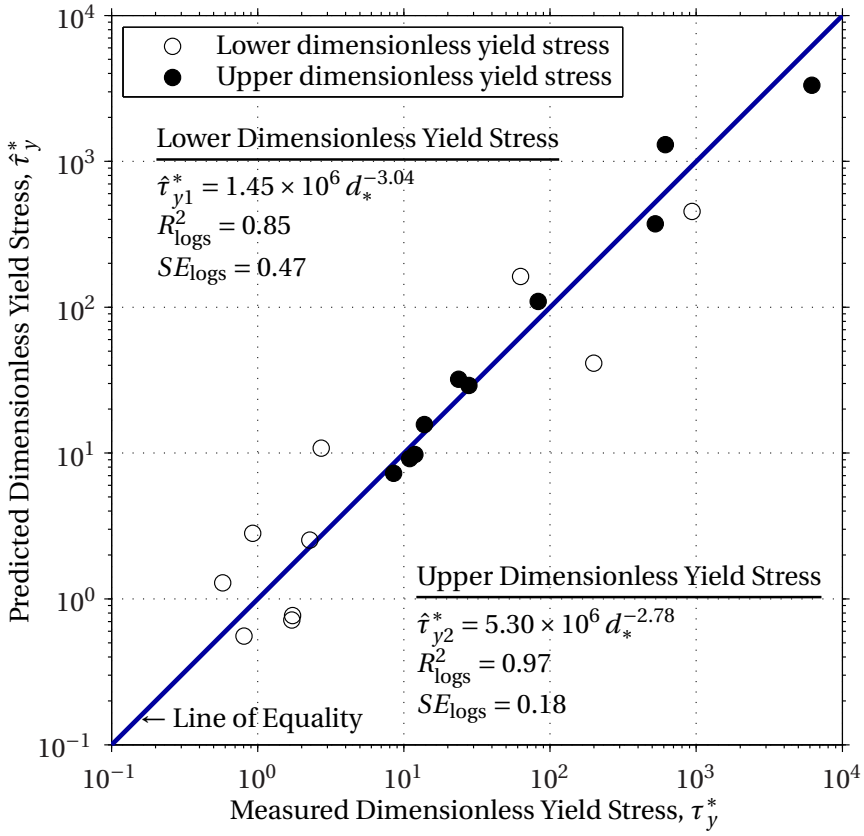

Figure 4.14: Predicting lower and upper dimensionless yield stress from dimensionless particle diameter

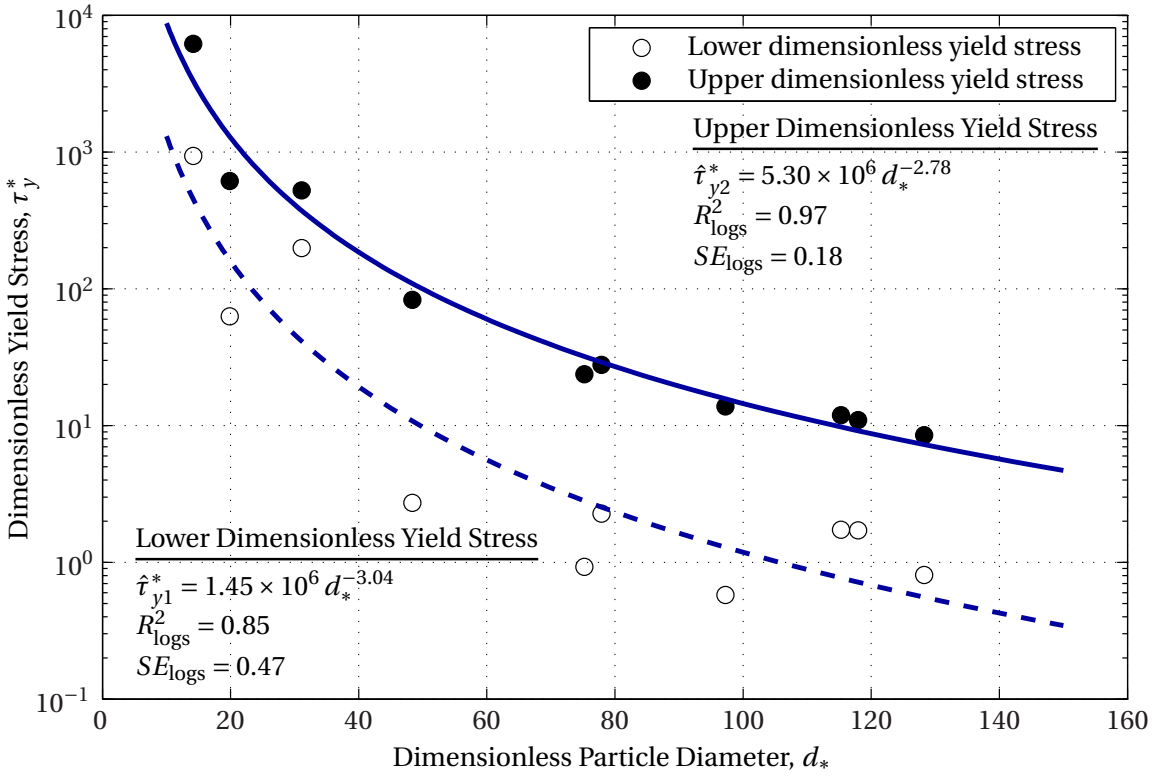

Figure 4.15: Predicting lower and upper yield stress from dimensionless particle diameter

from the lower and upper dimensionless yield stresses, respectively.

$$\hat{\tau}_{*c} = 0.644 \times 10^{2.48\text{Fines}} \left(\frac{\tau^*_{y1}}{1.45 \times 10^6} \right)^{0.134} \tag{4.20}$$

$$\hat{\tau}_{*c} = 0.644 \times 10^{2.48\text{Fines}} \left(\frac{\tau^*_{y2}}{5.30 \times 10^6} \right)^{0.147} \tag{4.21}$$

The primary difference between Equations 4.20 and 4.21 is the scaling factor applied to the dimensionless yield stress. The exponents applied to $\hat{\tau}^*_y$ are similar, 0.134 vs. 0.147, indicating a fairly consistent relationship between lower and upper dimensionless yield stresses. Equations 4.20 and 4.21 allow the specific plastic characteristics of the type of clay present in the fines to be characterized in the determination of the critical Shields parameter. These equations provide an additional layer of information for determination of critical shear stress as part of the original objective of the research and they are a unique contribution of the present study.

CHAPTER V

CONCLUSIONS AND RECOMMENDATIONS

5.1 Conclusions

In this study, the critical shear stress, lower yield stress, and upper yield stress of Georgia sediments from five bridge foundations were measured. The sample locations were selected in a manner to investigate bridges that sustained damage during Tropical Storm Alberto in 1994 and to spatially complement the previous investigation of Navarro (2004). The critical shear stress was determined by measuring the erosion rates of soil extruded from Shelby tubes into a tilting, recirculating, rectangular flume. Of the eleven sediment cores received, three contained a total of five materials whose critical shear stress and geotechnical characteristics could be determined. Following the erosion and geotechnical analyses, the fines (particles smaller than 75 μm) of any material exhibiting plastic characteristics were isolated by wet sieving over the No. 200 sieve. The upper and lower yield stresses of the fines were then determined from flow curves measured at various water contents using a stress controlled rheometer.

The critical shear stress data obtained during this study complement well the work of previous investigators (Navarro, 2004). The data reinforce the validity of the previously developed model used to predict the critical shear stress of a sediment based on its median particle size (d_{50}), fines content, and organic matter content. Additionally, both datasets together lead to the selection of an improved model used to predict the Shields parameter of a sediment based solely on the fines content. However, the recommended

relationship to be used is Equation 4.12 in which the critical value of the Shields parameter depends on a dimensionless value of the median particle diameter and the proportion of fine sediment (silt and clay) by weight in the size distribution as a decimal fraction. This relationship is limited to the sediment sizes and fines contents for the Georgia soils that were sampled, but it includes the data from this study as well as the data from the study by Navarro (2004). It includes both the viscous effects of the flow and the effect of the strength of the interparticle forces using the fraction of fine sediment as a surrogate.

For most samples containing a large portion of fines, two yield stresses were identified. The first and lower yield stress was obtained by finding the intersection of curves fit to the stress-strain flow curve to determine when the slurry started to appreciably flow. The upper yield stress was obtained from the intersection of two lines fit to the strain rate-stress data. The upper values were typically greater than the lower values by between a factor of 2 and an order of magnitude. Using these values, a new dimensionless yield stress was defined in a similar manner to the Shields parameter calculated from the critical shear stress. The dimensionless yield stresses correlate well with the dimensionless particle diameter. Because both the dimensionless yield stress and the Shields parameter depend on d_*, they must depend on each other and so Equations 4.20 and 4.21 were derived on this basis. Equations 4.20 and 4.21 allow the specific cohesive characteristics of the type of clay present in the fines to be characterized by the yield stresses in the determination of the critical Shields parameter. These equations provide an additional layer of information for determination of critical shear stress as part of the original objective of the research and they are a unique contribution of the present study.

5.2 Future Modifications to the Procedure

In addition to the modifications proposed by Navarro (2004), expanding the range of applied bed shear stresses obtainable in the recirculating flume would be the single greatest improvement to the procedure and apparatus. Of the 15 materials present and characterized in the Shelby tube samples received from GDOT, eight have critical shear stresses reported as >21 Pa. In other words, over half of the dataset is out of range for the flume. In all likelihood, enclosing and pressurizing the flume such that the maximum applied shear stress is over 75 Pa would have enabled most of these samples to be eroded, though similarity of the turbulence characterisics may be lost in the switch from free surface flow to enclosed conduit flow. With the greater ability to collect critical shear stress data, the possible relationships between yield stress and critical shear stress could be explored beyond the work of Hoepner (2000) and the work of this investigation. The most attractive benefit of developing such a relationship would be to accurately estimate the critical shear stress of sediments from bridge foundations using only yield stress data, which is obtained from a more robust, repeatable, and operator-independent experiment that requires roughly 30 g of fines per test. This could greatly advance the state of the practice of bridge foundation design as erosion characteristics of the foundation's sediments could be quickly and easily quantified with minimal sampling and quick laboratory turn around. This thesis has shown how such a relationship can be developed, although additional data are needed to make it more robust.

Along similar lines, improved sampling methods should be employed. It would be ideal if the samples could come directly from the bridge piers or at least the main channel of the stream. Failing those options, even the lower banks of the stream, where accessible, would be preferred. Judging from the few boring logs provided by GDOT, the samples received during this study were collected high in the floodplain. As a result, it is likely that these are not necessarily representative of the sediments found below the bridge

foundations.

5.3 Future Work

Future work in this subject area should continue to build upon the work of this study and those of Navarro (2004) and Hoepner (2000). Any continued work should include statistical analysis methods designed for dealing with censored datasets such as those presented in Helsel and Hirsch (2002) and Helsel (2005). Though it is currently beyond the scope of this project, there is yet much information to be gathered from the censored data regarding the sediment characteristics that determine the critical shear stress. Moreover, relationships between the critical shear stress and the yield stresses as developed in this study should be investigated in more detail. Artificially mixed soils would provide an excellent starting point for such a task.

References

Aberle, J., Nikora, V., McLean, S., Doscher, C., McEwan, I., Green, M., Goring, D., and Walsh, J. (2003). Straight benthic glow-through flume for *in situ* measurement of cohesive sediment dynamics. *Journal of Hydraulic Engineering*, 129(1):63–67.

Aberle, J., Nikora, V., and Walters, R. (2004). Effect of bed material properties on cohesive sediment erosion. *Marine Geology*, 207(1-4):83–93.

Aberle, J., Nikora, V., and Walters, R. (2006). Data interpretation for *in situ* measurements of cohesive sediment erosion. *Journal of Hydraulic Engineering*, 132(6):581–588.

Alhadeff, S. J., Musser, J. W., Sandercock, A. C., and Dyer, T. R. (2000). Digital Environmental Atlas of Georgia. 2 Disks.

Ansari, S. A., Kothyari, U. C., and Raju, K. G. R. (2003). Influence of cohesion on scour under submerged circular jets. *Journal of Hydraulic Engineering*, 129(12):1014–1094.

Bagnold, R. A. (1954). Experiments on a gravity-free dispersion of large soild spheres in a Newtonian fluid under shear. *Proceedings of the Royal Society of London*, 225:49–63.

Barry, K. M., Thieke, R. J., and Mehta, A. J. (2006). Quasi-hydrodynamic lubrication effect of clay particles on sand grain erosion. *Estuarine, Coastal and Shelf Science*, 67(1-2):161–169.

Black, K. S. (2002). Working with natural cohesive sediments. *Journal of Hydraulic Engineering*, 128(1):2–8.

Brandimarte, L., Montanari, A., Briaud, J. L., and D'Odorico, P. (2006). Stochastic flow analysis for predicting river scour of cohesive soils. *Journal of Hydraulic Engineering*, 132(5):493–500.

Briaud, J. L., Ting, F. C. K., Chen, H. C., Cao, Y., Han, S. W., and Kwak, K. W. (2001). Erosion function apparatus for scour rate predictions. *Journal of Geotechnical and Geoenvironmental Engineering*, 127(2):105–113.

Briaud, J. L., Ting, F. C. K., Chen, H. C., Gudavalli, R., Perugu, S., and Wei, G. (1999). Sricos: Prediction of scour rate in cohesive soils at bridge piers. *Journal of Geotechnical and Geoenvironmental Engineering*, 125(4):237–246.

Brownlie, W. R. (1981). Prediction of flow depth and sediment discharge in open channels. Technical Report KH-R-43A, W.M. Keck Laboratory of Hydraulics and Water Resources, California Institute of Technology, Pasadena, CA.

Budhu, M. (2000). *Soil Mechanics and Foundations*. John Wiley & Sons, Hoboken, NJ, first edition.

Debnath, K., Nikora, V., Aberle, J., Westrich, B., and Muste, M. (2007a). Erosion of cohesive sediments: Resuspension, bed load, and erosion patterns from field experiments. *Journal of Hydraulic Engineering*, 133(5):508–520.

Debnath, K., Nikora, V., and Elliott, A. (2007b). Stream bank erosion: *In situ* flume tests. *Journal of Irrigation and Drainage Engineering*, 133(3):256–264.

Dey, S. and Westrich, B. (2003). Hydraulics of submerged jet subject to change in cohesive bed geometry. *Journal of Hydraulic Engineering*, 129(1):44–53.

Donat, J. (1929). Uber Sohlangriff und Geschiebetrieb. *Wasserwirtschaft*, 26:27.

Dong, P. (2007). Two-fraction formulation of critical shear stresses for sand and silt mixtures. *Journal of Waterway, Port, Coastal, and Ocean Engineering*, 133(3):238–241.

Federico, V. D. (1999). Free-surface flow of hyperconcentrations. *Fluids Dynamics Research*, 24(1):23–26.

Fell, R., MacGregor, P., Stapledon, D., and Bell, G. (2005). *Geotechnical Engineering of Dams*, pages 302–303. Taylor & Francis Group, plc, London.

Ganaoui, O. E., Schaalf, E., Boyer, P., Amielh, M., Anselmet, F., and Grenz, C. (2007). Erosion of the upper layer of cohesive sediments: Characterization of some properties. *Journal of Hydraulic Engineering*, 132(9):1087–1091.

Gerbersdorf, S. U., Jancke, T., and Westrich, B. (2006). Sediment properties for assessing the erosion risk of contaminated rivers. *Journal of Soils and Sediments*, 7(1):25–37.

Helsel, D. R. (2005). *Nondetects and Data Analysis: Statistics for Censored Environmental Data*. Statistics in Practice. John Wiley & Sons, Hoboken, NJ.

Helsel, D. R. and Hirsch, R. M. (2002). *Statistical Methods in Water Resources*. Number 4 in Techniques of Water Resources Investigations. United States Geologic Survey.

Hoepner, M. A. (2000). Stability of cohesive sediments from flume and rheometer measurements. Master's thesis, Georgia Institute of Technology.

Julien, P. Y. (1995). *Erosion and Sedimentation*. Cambridge University Press, New York.

Julien, P. Y. and Lan, Y. (1991). Rheology of hyperconcentrations. *Journal of Hydraulic Engineering*, 117(3):346–353.

Krishnappan, B. G. (2007). Recent advances in basic and applied research in cohesive sediment transport in aquatic systems. *Canadian Journal of Civil Engineering*, 34(6):731–743.

Krone, R. B. (1999). Effects of bed structure on erosion of cohesive sediments. *Journal of Hydraulic Engineering*, 125(12):1297–1301.

Laird, W. M. (1957). Slurry and suspension transport: Basic flow studies on Bingham plastic fluids. *Industrial and Engineering Chemistry*, 49(1):138 – 141.

Lee, S. C., Mehta, A. J., and Parchure, T. M. (1994a). Cohesive sediment erosion: Part 1, Test devices and field instruments assemblies. Internal report, Coastal and Oceanographic Engineering Department, University of Florida, Gainesville, Florida.

Lee, S. C., Mehta, A. J., and Parchure, T. M. (1994b). Cohesive sediment erosion: Part 2, Relationship between the erosion rate constant and bed shear strength. Internal report, Coastal and Oceanographic Engineering Department, University of Florida, Gainesville, Florida.

Lick, W., Jin, L., and Gailani, J. (2004). Initiation of movement of quart particles. *Journal of Hydraulic Engineering*, 130(8):755–761.

Mahmood, T., Amirtharajah, A., Sturm, T. W., and Dennett, K. E. (2001). A micromechanics approach for attachement and detachment of asymnetric colloidal particles. *Colloids and Surfaces A: Physiochemical and Engineering Aspects*, 177(2):99–110.

Markovitz, H. (1985). Rheology: in the beginning. *Journal of Rheology*, 29(6):777–798.

Mazurek, K. A., Rajaratnam, N., and Sego, D. C. (2001). Scour of cohesive soil by submerged circular turbulent impinging jets. *Journal of Hydraulic Engineering*, 127(7):598–606.

McNeil, J., Taylor, C., and Lick, W. (1996). Measurements of erosion of undisturbed bottom sediments with depth. *Journal of Hydraulic Engineering*, 122(6):316–324.

Mehta, A. J. (1991). Review notes on cohesive sediment erosion. In Kraus, N. C., Gingerich, K. J., and Kriebel, D. L., editors, *Coastal Sediments*, volume 1, pages 40–53. American Society of Civil Engineers.

Mehta, A. J. (1994). Characterization of cohesive soil erosion with special reference to the relationship between erosion shear strength and bed density. Internal Report UFL/COEL/MP-91/4, Coastal and Oceanographic Engineering Department, University of Florida, Gainesville, Florida.

Mitchell, J. K. and Soga, K. (2005). *Fundamentals of Soil Behavior*, chapter 4, pages 83–108. John Wiley & Sons, Hoboken, NJ, third edition.

Navarro, H. R. (2004). Flume measurements of erosion characteristics of soils at bridge foundations in Georgia. Master's, Georgia Institute of Technology.

Nguyen, Q. D. and Boger, D. V. (1992). Measuring the flow properties of yield stress fluids. *Annual Reviews: Fluid Mechanics*, 24(1):47–88.

O'Brien, J. S. and Julien, P. Y. (1988). Laboratory analysis of mudflow properties. *Journal of Hydraulic Engineering*, 114(8):877–887.

Otsubo, K. and Muraoka, K. (1988). Critical shear stress of cohesive bottom sediments. *Journal of Hydraulic Engineering*, 114(10):1241–1256.

Panagiotopoulos, I., Voulgaris, G., and Collins, M. B. (1997). The influence of clay on the threshold of movement of fine sandy beds. *Coastal Engineering*, 32(1):19–43.

Partheniades, E. (1965). Erosion and depostion of cohesive soll. *Journal of Hydraulic Engineering*, 91(1):105–139.

Paterson, D. M. (1989). Short term changes in the erodibility of intertidal cohesive sediments related to the migratory behaviour of epipelic diatoms. *Limnology and Oceanography*, 34(1):223–234.

Ravens, T. M. (2007). Comparison of two techniques to measure sediment erodibility in ithe Fox River, Wisconson. *Journal of Hydraulic Engineering*, 133(1):111 – 115.

Ravens, T. M. and Gschwend, P. M. (1999). Flume measurements of sediment erodibility in boston harbor. *Journal of Hydraulic Engineering*, 125(10):998–1005.

Ravisangar, V., Dennett, K. E., Sturm, T. W., and Amirtharajah, A. (2001). Effect of sediment pH on resuspension of kaolinite sediments. *Journal of Environmental Engineering*, 127(6):531–538.

Ravisangar, V., Sturm, T. W., and Amirtharajah, A. (2005). Influence of sediment structure on erosional strength and density of kaolinite sediment beds. *Journal of Hydraulic Engineering*, 131(5):356–365.

Richardson, E. V. and Davis, S. R. (2001). Evaluating scour at bridges. Technical Report FWHA NHI 01-001 HEC-18, Federal Highway Administration and Nation Highway Institute.

Roberts, J., Jepsen, R., Gotthard, D., and Lick, W. (1998). Effect of particle size and bulk density on erosion of quartz particles. *Journal of Hydraulic Engineering*, 124(12):1261–1267.

Roberts, J. D., Jepsen, R. A., and James, S. C. (2003). Measurement of sediment erosion and transport with the adjustable shear stress erosion and transoport flume. *Journal of Hydraulic Engineering*, 129(11):862–971.

Santamarina, J. C. (2001). Soil behavior at the microscale: Particle forces. *Proc. Symp. Soil Behavior and Soft Ground Construction, in honor of Charles C. Ladd*, pages 1–32.

Shields, A. (1936). Applications of similarity principles and turbulence research to bedload movement. Hydrodynamics Laboratory Publication 167, USDA, Soil Conservation Service Cooperative Laboratory, California Institute of Technology, Pasadena, CA.

Shugar, D., Kostaschuk, R., Ashmore, P., Desloges, J., and Burge, L. (2007). In situ jet-testing of the erosional resisticance of cohesive streambeds. *Canadian Journal of Civil Engineering*, 34(9):1192–1195.

Sturm, T. W. (2001). *Open Channel Hydraulics*. Textbook series in water resources and environmental engineering. McGRaw Hill, New York, second edition.

Ting, F. C. K., Briaud, J. L., Chen, H. C., Gudavalli, R., Perugu, S., and Wei, G. (2001). Flume test for scour in clay at circular piers. *Journal of Hydraulic Engineering*, 127(11):969–978.

Tolhurst, T. J., Black, K. S., Shayler, S. A., Mather, S., Black, I., Baker, K., and Paterson, D. M. (1999). Measuring the *in situ* erosion shear strength of intertidal sediments with cohesive strength meter (CMS). *Estuarine, Coastal and Shelf Science*, 49(2):281–294.

Torfs, H. (1995). *Erosion of sand/mud mixtures*. Ph.D. dissertation, Katholieke Universiteit Leuven, Leuven, The Netherlands.

van Kessel, T. (1998). Rheology of cohesive sediments: Comparison between a natural and an artificial mud. *Journal of Hydraulic Research*, 36(4):591–612.

van Olphen, H. (1977). *An Introduction to Clay Colloid Chemistry*. John Wiley & Sons, New York, second edition.

Watts, C. W., Tolhurst, T. J., Black, K. S., and Whitmore, A. P. (2003). *In situ* measurements of erosion shear stress and geotechnical shear strength of the intertidal sediments of the experimental managed realignment scheme at Tollesbury, Essex, Uk. *Estuarine, Coastal and Shelf Science*, 58(3):611–620.

Witt, O. and Westrich, B. (2003). Quantification of erosion rates for undisturbed contaminated cohesive sediment cores by image analysis. *Hydrobiologia*, 494(1-3):271–276.

Wright, V. G. and Krone, R. B. (1987). *Laboratory Study of Mud Flows*. American Society of Civil Engineers, New York.

Zreik, D. A., Krishnappan, B. G., Germaine, J. T., Madsen, O. S., and Ladd, C. C. (1998). Erosional and mechanical strengths of deposited cohesive sediments. *Journal of Hydraulic Engineering*, 124(11):1076–1085.